INTERFACE

rsif.royalsocietypublishing.org

Headline review

Cite this article: Alevriadou BR, Shanmughapriya S, Patel A, Stathopulos PB, Madesh M. 2017 Mitochondrial Ca^{2+} transport in the endothelium: regulation by ions, redox signalling and mechanical forces. *J. R. Soc. Interface* **14**: 20170672.
http://dx.doi.org/10.1098/rsif.2017.0672

Received: 13 September 2017
Accepted: 16 November 2017

Subject Category:
Reviews

Subject Areas:
synthetic biology, bioenergetics, bioengineering

Keywords:
mitochondria, mitochondrial Ca^{2+} uniporter, reactive oxygen species, vascular endothelial cell, shear stress, atherosclerosis

Authors for correspondence:
B. Rita Alevriadou
e-mail: rita.alevriadou@osumc.edu
Peter B. Stathopulos
e-mail: peter.stathopulos@schulich.uwo.ca
Muniswamy Madesh
e-mail: madeshm@temple.edu

THE ROYAL SOCIETY PUBLISHING

Mitochondrial Ca^{2+} transport in the endothelium: regulation by ions, redox signalling and mechanical forces

B. Rita Alevriadou[1,2,3], Santhanam Shanmughapriya[4,5], Akshar Patel[1,2,3], Peter B. Stathopulos[6] and Muniswamy Madesh[4,5]

[1]Department of Biomedical Engineering, and [2]Department of Internal Medicine, Division of Cardiovascular Medicine, and [3]Davis Heart and Lung Research Institute, The Ohio State University, Columbus, OH 43210, USA
[4]Department of Medical Genetics and Molecular Biochemistry, and [5]Center for Translational Medicine, Lewis Katz School of Medicine, Temple University, Philadelphia, PA 19140, USA
[6]Department of Physiology and Pharmacology, Western University, London, Ontario, Canada N6A 5C1

BRA, 0000-0003-1897-755X; PBS, 0000-0002-0536-6656; MM, 0000-0001-6745-9092

Calcium (Ca^{2+}) transport by mitochondria is an important component of the cell Ca^{2+} homeostasis machinery in metazoans. Ca^{2+} uptake by mitochondria is a major determinant of bioenergetics and cell fate. Mitochondrial Ca^{2+} uptake occurs via the mitochondrial Ca^{2+} uniporter (MCU) complex, an inner mitochondrial membrane protein assembly consisting of the MCU Ca^{2+} channel, as its core component, and the MCU complex regulatory/auxiliary proteins. In this review, we summarize the current knowledge on the molecular nature of the MCU complex and its regulation by intra- and extramitochondrial levels of divalent ions and reactive oxygen species (ROS). Intracellular Ca^{2+} concentration ($[Ca^{2+}]_i$), mitochondrial Ca^{2+} concentration ($[Ca^{2+}]_m$) and mitochondrial ROS (mROS) are intricately coupled in regulating MCU activity. Here, we highlight the contribution of MCU activity to vascular endothelial cell (EC) function. Besides the ionic and oxidant regulation, ECs are continuously exposed to haemodynamic forces (either pulsatile or oscillatory fluid mechanical shear stresses, depending on the precise EC location within the arteries). Thus, we also propose an EC mechanotransduction-mediated regulation of MCU activity in the context of vascular physiology and atherosclerotic vascular disease.

1. Introduction

The endothelium is a cellophane-like membrane lining the circulatory system and its major functions are regulation of vascular tone and vessel wall permeability. Endothelial cell (EC) dysfunction has been implicated in the early stages of many cardiovascular diseases, which renders the modulation of EC functions a key therapeutic target [1–3]. Under normal conditions, EC functions depend on changes in the intracellular calcium concentration ($[Ca^{2+}]_i$). The Ca^{2+} concentration in extracellular biological fluids is in the range of 1.6–2 mM, whereas, within cells, Ca^{2+} is bound to phospholipids, proteins and nucleic acids or is sequestered in organelles, and thus only 0.1% of the total Ca^{2+} content is free in the cytosol. Consequently, $[Ca^{2+}]_i$ is kept at approximately 100 nM to regulate cellular processes that function over a wide dynamic range. In most cells, increases in $[Ca^{2+}]_i$ are transient and oscillatory [4] and the frequency of oscillation (temporal $[Ca^{2+}]_i$ signature) is differentially decoded as cellular signal [5]. At any time, the spatio-temporal complexity in the regulation of $[Ca^{2+}]_i$ is determined by a balance between the interplay of multiple counteracting processes divided into 'on' and 'off' mechanisms. The 'on' reaction results in generation of the $[Ca^{2+}]_i$ rise due to Ca^{2+} influx from the extracellular medium and Ca^{2+} release from intracellular stores, such as the endoplasmic reticulum (ER) in non-excitable cells. The 'off' reaction removes intracellular Ca^{2+} by the combined action of pumps, buffers and exchangers. One important intracellular organelle associated with Ca^{2+} handling is the mitochondrion [6,7]. Although

other compartments such as the ER, lysosomes, Golgi apparatus and endosomes are recognized as Ca^{2+} stores [7–9], the mitochondria remain highly specialized in this context because of their sponge-like retentive capacity with regard to Ca^{2+}.

In ECs, the mitochondria account for 25% of the cell's Ca^{2+} storage. It has long been ascertained that mitochondrial content in ECs is modest (endothelial mitochondria occupy 2–6% of the cytoplasmic volume) compared with cardiac myocytes (32% of the cytoplasmic volume) and other cell types, as the energy requirements in ECs are relatively low and glycolysis is the major source of ATP production. *In vitro* and *in vivo* studies have shown that, apart from the well-known role of mitochondria in bioenergetics, they also play a prominent role in signalling cellular responses to environmental cues [10–12]. Two such important modes of signalling are their regulated production of mitochondrial reactive oxygen species (mROS) and their service as Ca^{2+} sinks. Mitochondrial Ca^{2+} uptake and mROS generation are interdependent phenomena and contribute to cell function in a 'mutual crosstalk', with mitochondrial Ca^{2+} concentration ($[Ca^{2+}]_m$) representing the key to deciphering mROS signals [13].

Mitochondria have a large negative membrane potential of 180 mV that facilitates flooding of mitochondria by Ca^{2+} from the cytosolic milieu. During evolution, cells acquired sophisticated mitochondrial Ca^{2+} transport machineries that control Ca^{2+} entry to the mitochondrial matrix and Ca^{2+} exit/redistribution for proper cell function. The mitochondrial Ca^{2+} uptake system is a heterogeneous protein complex with the molecular identity mixed and matched with the mitochondrial Ca^{2+} uniporter (MCU) as the core component [14,15]. The MCU is regulated by an array of proteins including mitochondrial Ca^{2+} uptake 1 (MICU1), 2 (MICU2), 3 (MICU3), essential MCU regulator (EMRE), MCU regulating protein 1 (MCUR1) and MCU dominant negative beta subunit (MCUb) (see §2 for a complete description) [16–24]. Besides protein regulation (positive by MCUR1 and EMRE [19,23] and negative by MICU1 [22]), recent studies from our group and others demonstrated a regulation of mitochondrial Ca^{2+} uptake by ions and redox signalling. In this review, we summarize these regulatory mechanisms of MCU activity and suggest a potential therapeutic utility in controlling endothelial MCU activity during vascular (patho)physiology. We also introduce a novel hypothesis that spatial regulation of MCU activity by local haemodynamic forces (via their effect on ion and redox signalling) in human arteries may, at least in part, explain the focal nature of atherosclerotic vascular disease. Since atherosclerotic vascular disease continues to be the major cause of death in developed nations [25] and EC dysfunction plays a causative role in disease initiation [26,27], this review aims to position the MCU as a potential critical target for intervention against atherosclerosis.

2. Ionic regulation of mitochondrial Ca^{2+} uptake

The MCU contains two transmembrane (TM) domains with coiled-coil regions positioned before and after these domains. Topologically, both the N- and C-terminal regions reside in the matrix constituting a majority of the protein [28]. The regulation of the MCU pore is complex as evidenced by the numerous protein regulators which have been identified. MCUb is a homologue of MCU sharing 50% sequence similarity, but no ability to constitute a Ca^{2+}-permeable channel despite the presence of similar TM domains to those found in the MCU. These MCUb TM domains contain two noteworthy amino acid substitutions (R251Q and D256V) compared with the MCU, which may be related to the dominant negative inhibition of MCU activity after interactions with MCUb [20]. MICU1/2/3 proteins play gating roles promoting a closed MCU at low $[Ca^{2+}]_i$ [19,21,23,24,29–33]. EMRE is a 10 kDa, single TM protein that stabilizes and/or bridges MCU and MICU1 interactions [19]. Solute carrier family 25 member 23 (SLC25A23) is found on the inner mitochondrial membrane (IMM) and functions as an ATP and phosphate transporter protein, interacting with both MCU and MICU1 and enhancing mitochondrial Ca^{2+} uptake [34]. MCUR1 is a 40 kDa protein containing two putative TM domains; moreover, it has recently been determined that MCUR1 is a vital scaffold factor required for assembly of the heteromeric MCU complex through interactions with both EMRE and the MCU [16,23].

The regulation of the MCU via its numerous protein binding partners has been delineated recently; however, the ability of $[Ca^{2+}]_i$ to regulate MCU channel activity was reported approximately 25 years prior to the identification of any of the genes/proteins involved in this process [35–38]. Furthermore, it is now clear that some of the protein regulators exert their modulatory function via interactions with Ca^{2+} ions. MICU1 is a 54 kDa protein that has two Ca^{2+} binding EF-hand domains. Vertebrates express three homologues, but only the functions of MICU1 and MICU2 appear non-redundant with respect to MCU regulation, while MICU3 is predominantly localized to the central nervous system [39]. Studies are in agreement about the gatekeeping function of MICUs at low $[Ca^{2+}]_i$, but localization within the mitochondria, sites of interaction with the MCU and function at higher $[Ca^{2+}]_i$ have been debated [19,21,23,29–32]. Knockdown of MICU1 causes augmented $[Ca^{2+}]_m$ at basal $[Ca^{2+}]_i$ [23,30] due to destabilization of the MICU1 homologue, MICU2, which inhibits MCU channel activity [18]; moreover, MICU1 overexpression in MICU2-depleted cells also increases $[Ca^{2+}]_m$, suggesting that MICU1 is a stimulator of MCU uptake [18]. MICU1 has been reported to be mitochondrial matrix localized, directly interacting with the MCU [21], or intermembrane space localized, indirectly interacting with the MCU via an accessory protein [30,40]. Knockout of MICU1 results in unregulated MCU activity, while knockout of MICU2 only lowers the Ca^{2+} level threshold at which MICU1 gates the MCU; moreover, the MICU1 or MICU2 Ca^{2+} binding-incompetent mutants constitutively inactivate the MCU irrespective of Ca^{2+} levels [31]. Recently, it has been demonstrated that MICU1–MICU2 heterodimer formation establishes a steeply cooperative sub-micromolar Ca^{2+} binding affinity; moreover, the sharp Ca^{2+}-binding cooperativity conveys a binary-like ON/OFF MCU activation phenotype over relatively small changes in $[Ca^{2+}]_i$ [36].

A crystal structure of MICU1 revealed that two EF-hand pairs (i.e. EF1 and EF2) are each preceded by intervening domains (i.e. ID1 and ID2) (figure 1*a*). Structural homology analysis using DALI [41,42] shows that no other currently known structure arranges EF-hand domains with similar ID1/2 structures. While EF1/2 show significant homology to calmodulin (CaM)-like proteins, ID1/2 appear relatively unique. Each EF-hand pair coordinates a single Ca^{2+} ion resulting in increased interhelical angles [43], yet the clefts do not show any evidence for intramolecular or homotypic intermolecular protein interactions in the available structures, contrary to other EF-hand proteins [44–48]. Furthermore, structural

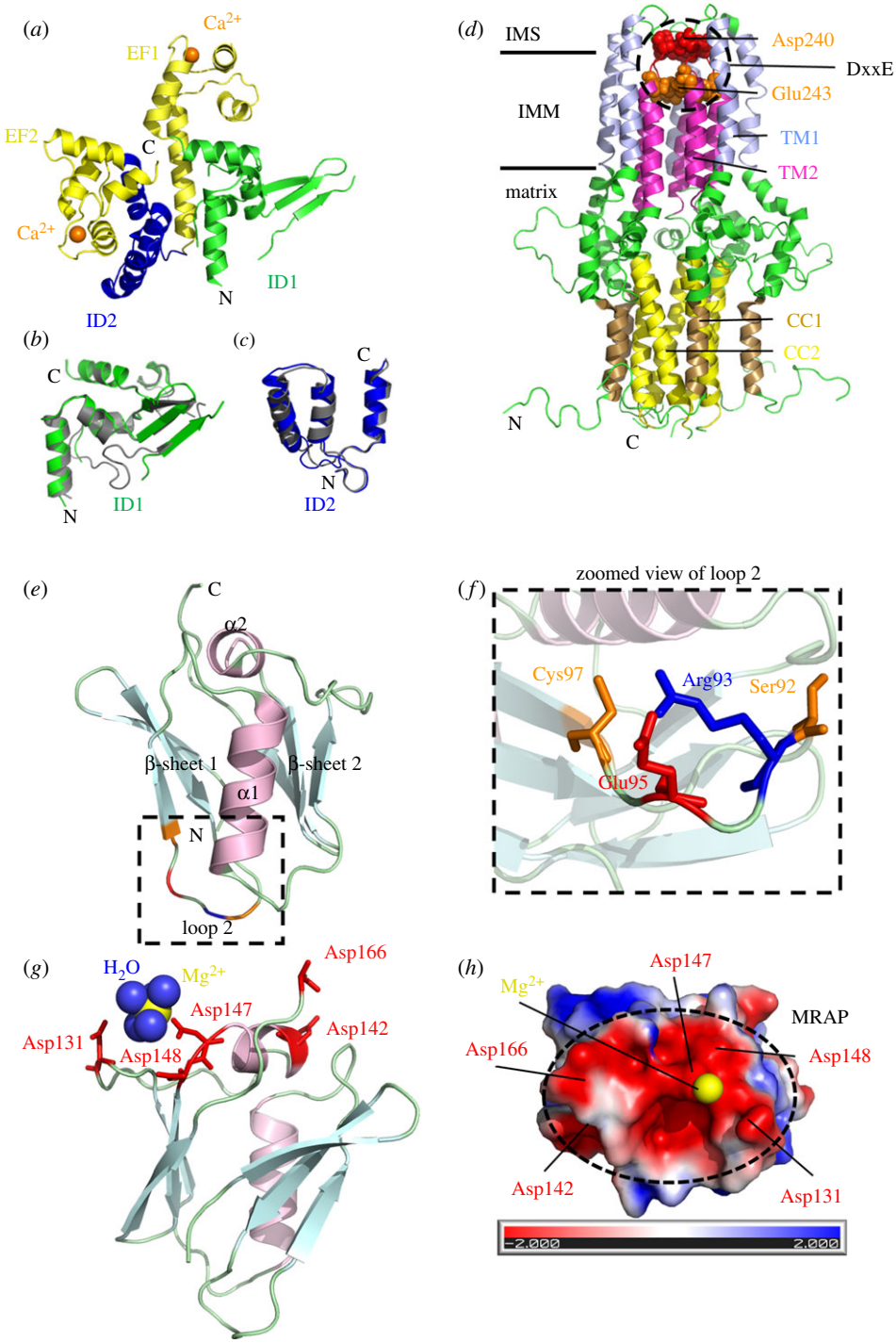

Figure 1. Structural mechanisms of MCU regulation. (*a*) Crystal structure of human MICU1 residues 108–442 in the Ca^{2+}-bound state. The conformation and orientation of the two EF-hand domains (yellow ribbon diagrams; EF1 (residues 219–315); EF2 (residues 374–442)) are shown relative to the two preceding intervening domains (ID1, green ribbon diagram (residues 108–218); ID2, blue ribbon diagram (residues 316–373)). Each EF-hand domain coordinates a single Ca^{2+} atom (orange spheres). (*b*) All-atom structural alignment of the MICU1 ID1 domain in the presence (green ribbon) and absence (grey ribbon) of Ca^{2+}. (*c*) All-atom structural alignment of the MICU1 ID2 domain in the presence (blue ribbon) and absence (grey ribbon) of Ca^{2+}. ID1 and ID2 adopt similar structures with the EF-hand domains in either an open or a closed conformation. (*d*) NMR- and transmission electron microscopy-driven model of the *Caenorhabditis elegans* C-terminal domain residues 166–318. The inner pore is made up of TM2 (magenta ribbons; residues 244–260) and is surrounded by TM1 (light blue ribbons; residues 215–234). The DXXE motif (dashed black circle) links TM1 and TM2. The Asp240 (red space fill) and Glu243 (orange space fill) residues which bind Mn^{2+} cooperatively are indicated within the DXXE motif. The outer and inner coiled-coil bundles (CC1, brown ribbons (residues 180–193); CC2, yellow ribbons (293–316)) are labelled. The location of the matrix, IMM and IMS are shown relative to the TM domains. (*e*) Crystal structure of the human MCU N-terminal domain residues 72–189. The two β-sheets (light blue ribbons; residues 76–80, 83–88, 97–100 for β-sheet 1 and 125–128, 149–153, 156–160 for β-sheet 2) grasping the two centrally located helices (pink ribbons; residues 108–118 and 141–146 for α1 and α2, respectively) are labelled. The dashed black box highlights the location of the loop 2. (*f*) Zoomed view of the Cys97 and Ser92 residues within loop 2 which are susceptible to post-translational modifications. The close spatial proximity of the Arg93 and Glu95 side chains which form a salt bridge in some of the crystallized forms and stabilize the loop is shown. (*g*) First shell ligand coordination of the Mg^{2+} atom (yellow sphere) by the Asp147 side chain and five H_2O molecules (blue spheres) in an octahedral geometry. The close spatial proximity of the other Asp residues making MRAP are also indicated (red sticks). (*h*) Electrostatic surface potential of the human MCU N-terminal domain residues 72–189. The large MRAP region is indicated by a dashed black circle, and the individual acidic residues contributing to the region are labelled relative to the Mg^{2+} atom (yellow sphere). The −2 (red) to +2 (blue) kT/e gradient is shown below the protein. In (*a–h*) amino and carboxy termini are labelled N and C, respectively. The structures were rendered in PyMOL using the 4NSD (Ca^{2+}-loaded) and 4NSC (Ca^{2+}-depleted) coordinates for MICU1, 5ID3 for the *C. elegans* MCU C-terminal domain and 5KUJ for the human MCU N-terminal domain.

alignment of ID1/2 domains when EF1/2 are in the Ca^{2+}-loaded and -depleted states show only minor structural differences (figure 1*b*,*c*). Thus, the structural mechanisms underlying MICU1 modulation of MCU activity and how Ca^{2+} may affect this regulation remain unclear.

Many Ca^{2+} channel proteins exhibit Ca^{2+}-dependent feedback mechanisms including the inositol 1,4,5-trisphosphate receptor (IP_3R) [49,50], ryanodine receptor [51] and Ca^{2+} release-activated Ca^{2+} channel [52,53]. In the seminal work by Kirichok *et al.* [54], which first characterized the electrophysiological properties of the MCU channel using mitoplast patch clamp recordings, no Ca^{2+}-dependent inactivation was evident between 0.01 and 10 µM intramitoplast Ca^{2+} concentration at constant energy potentials of −160 mV. However, the same study demonstrated greater than 50% reduction in the Ca^{2+} conductance of the MCU in a 0.2 mM Ca^{2+}/0.5 mM Mg^{2+} extramitochondrial divalent cation mixture [54]. Additionally, numerous studies have described different aspects of Ca^{2+}-dependent MCU inactivation over the past decades, even prior to the molecular identification of the MCU complex components (e.g. [38,55–58]). More recently, however, a report has suggested that the C-terminal domain of EMRE is responsible for a matrix Ca^{2+}-dependent inactivation phenomenon at low $[Ca^{2+}]_i$. Using mitoplast patch clamp experiments, raising matrix Ca^{2+} concentrations to between approximately 0.03 and 0.4 µM markedly inhibited inward rectifying uniporter currents [59]. Consistent with this notion, mutations or truncations within the EMRE C-terminal domain abolished this Ca^{2+}-dependent inactivation phenomenon [59]. However, given that the topology of EMRE remains controversial with several papers suggesting that the C-terminal domain lies in the inner membrane space (not the matrix) [16,60,61], the precise molecular mechanisms behind Ca^{2+}-dependent MCU inactivation mediated by low matrix Ca^{2+} concentration effects on EMRE remain to be clarified.

Although a high-resolution structure of the pore-forming and coiled-coil regions of human MCU is currently unavailable, a nuclear magnetic resonance (NMR) spectroscopy- and transmission electron microscopy-driven pentameric model of *Caenorhabditis elegans* MCU with a deleted N-terminal domain has been constructed [62]. This structure shows that the second TM domain is positioned to line the pore of the channel with a short DXXE motif contributed by each subunit lining the entrance to the pore (figure 1*d*). The DXXE motif links the first and second TM domains. While the Glu is positioned deeper in the pore, the Asp is more solvent exposed, and mutating either of these acidic residues abrogates MCU channel activity [14]. NMR titrations showed that this DXXE motif can bind Mn^{2+}, a surrogate for Ca^{2+}-binding in NMR titrations, at both the Asp and Glu residues in a cooperative manner [63]. This strongly positive binding cooperativity for Ca^{2+} (i.e. defined by surrogate Mn^{2+} binding experiments) may underlie the ion selectivity mechanism of the MCU. This same site is involved in binding ruthenium red MCU channel inhibitors at the more exposed Asp residues [63], thus blocking the pore entrance.

While the C-terminal region alone can assemble and form an active channel [62], the significance of the N-terminal domain for the regulation of the channel is evident from work showing that self-association of the N-terminal half of the MCU promotes channel assembly and activation [64], oxidative modification of C97 within this N-terminal domain alters the channel architecture and function (see §3 for a complete description) [65], and the S92A mutation in this N-terminal domain dominant negatively disrupts mitochondrial Ca^{2+} uptake in cells [66]. Thus, the MCU N-terminal domain appears to serve as an important sensory hub which regulates MCU channel activity. Several high-resolution crystal structures of the human MCU N-terminal domain have been elucidated in the presence of various ions and concentrations (i.e. see PDB codes 5KUG, 5KUE, 5KUI, 5KUJ, 4XTB, 5BZ6, 4XSJ) [64,66]. The human MCU N-terminal domain forms a β-grasp-like fold made up of two three-stranded β-sheets holding two centrally located α-helices (figure 1*e*). The shorter α2-helix sits as a cap on the overall globular fold and is arranged approximately perpendicular to the central α1-helix. Interestingly, the extended loop 2, which connects the β1- and β2-strands and contains the S92 and C97 residues previously found to regulate channel activity by phosphorylation [66,67] and S-glutathionylation (SSG) [65], respectively, also contains a salt bridge which stabilizes this functionally important loop (figure 1*f*). The salt bridge is not present in all crystal forms, suggesting that local environmental conditions, including ionic strength, can modulate the structure and stability of the loop and, thus, the post-translational modifications which regulate channel activity.

The surface electrostatic potential of the MCU N-terminal domain forms two negatively charged acidic and two positively charged basic patches. The largest acidic patch is near the C-terminal region of the domain and is primarily constituted by D131, D142, D147, D148 and D166 residues (figure 1*g*). These acidic residues are conserved among vertebrate MCU homologues, suggesting an important role affiliated with the surface exposure. Indeed, Mg^{2+} ion has been found bound to this acidic patch in one crystal form [64]. The first shell Mg^{2+} coordination to the protein occurs through a D147 side chain oxygen atom, although the D131 and D148 side chains are also located within approximately 6.5 Å of the ion. The octahedral coordination geometry occurs via ligating of five additional water molecules, two of which are bridged by D123 side chain oxygens in second shell coordination (figure 1*h*). The single-ligand first shell and double-ligand second shell coordination interactions with the protein are consistent with the weak Mg^{2+} binding (i.e. approx. millimolar affinity) estimated using *in vitro* experiments with the isolated N-terminal domain in solution [64]. Ca^{2+} was also found to interact weakly with the N-terminal domain in solution using a similar assessment.

While the MCU N-terminal domain crystallized as a monomer, solution investigations by analytical ultracentrifugation and size-exclusion chromatography with inline multi-angle light scattering showed that the domain self-associates. Remarkably, inclusion of Ca^{2+} or Mg^{2+} divalent cations in the experimental buffers shifted the self-association equilibrium towards the monomer and, consistently, destabilized the fold. Furthermore, D131R or D147R charge swapping mutations caused a similar shift in the self-association equilibrium towards the monomer as the divalent cations [64]. Thus, incorporation of a basic residue in the acidic patch by mutation mimics the effects of basic cation coordination in this region of the MCU N-terminal domain. To assess the functional significance of this acidic patch, these mutations were also incorporated into constructs expressing full-length human MCU. In HeLa cells, expression of full-length human MCU harbouring D131R or D147R mutations caused a profound dominant negative inhibition of mitochondrial Ca^{2+} uptake without altering the IMM potential [64]. Furthermore, as observed in the isolated MCU N-terminal domain context,

the mutations perturbed the full-length assembly of the protein complex. Consistent with the mutational phenotypes, blockade of Ca^{2+} extrusion from the matrix using a Na^+/Ca^{2+} exchange inhibitor significantly decreased the Ca^{2+} uptake rates after a series of $[Ca^{2+}]_i$ pulses. With each successive $[Ca^{2+}]_i$ pulse, the matrix underwent loading concomitant with decreased mitochondrial Ca^{2+} uptake rates. Importantly, the membrane potential remained intact during this pulse train. Congruently, incubation with extramitochondrial Mg^{2+}, which is taken up into the matrix via the Mrs2p channel, also significantly decreased mitochondrial Ca^{2+} uptake rates [64]. Collectively, these data identified an MCU regulating acidic patch (MRAP) on the conserved MCU N-terminal domain which binds Mg^{2+} and Ca^{2+}, resulting in a destabilization of the self-association equilibrium and perturbation of the full-length MCU complex assembly. Ultimately, this divalent cation-induced perturbation in functional MCU architecture represents an autoregulation mechanism for physiologically vital cellular processes. The weak Mg^{2+} binding affinity of the MCU N-terminal domain is in the range of Mg^{2+} concentrations reported in the matrix and, thus, ideally suited as a sensor of Mg^{2+} levels which would be affected by Mrs2p activity as well as the metabolic state of the cell (i.e. ADP, ATP and PO_4^{3-} levels) [68,69]. On the other hand, the Ca^{2+} binding sensitivity of the MCU N-terminal would depend on a close proximity of the MCU N-terminal domain to the channel pore, where approximately millimolar levels may be reached in nanodomains [70–72]. Future high-resolution structural information of the intact human MCU protein is required to precisely capture the atomic mechanism for transduction from the disruption of the N-terminal domain self-association equilibrium to inhibition of MCU channel activity.

3. Regulation of mitochondrial Ca^{2+} transport by redox signalling

In agonist-stimulated non-excitable cells, it is generally accepted that $[Ca^{2+}]_i$ oscillations are triggered by Ca^{2+} release from the ER IP_3R and are fine-tuned by repetitive Ca^{2+} exchange between ER and the mitochondria, but they also depend on store-operated Ca^{2+} entry for long-term sustainability [7,73,74]. Specifically, following the binding of a cytokine to its G protein-coupled receptor (GPCR) on the plasma membrane, GPCR activates phospholipase C (PLC), which hydrolyses phosphatidylinositol 4,5-bisphosphate (PIP_2) to IP_3 and diacylglycerol (DAG) (figure 2*a*) [77]. IP_3 activates its receptor on the ER and promotes Ca^{2+} release [77] (figure 2*a*). In addition to regulation by IP_3, IP_3R is regulated by Ca^{2+} in a biphasic manner; low $[Ca^{2+}]_i$ stimulates IP_3R, whereas high $[Ca^{2+}]_i$ inhibits ER Ca^{2+} release [78,79]. Store depletion activates store-operated Ca^{2+} channels on the plasma membrane allowing Ca^{2+} influx from the extracellular space [77]. The mitochondria release some of their Ca^{2+} via the mitochondrial Na^+/Ca^{2+} exchanger (mNCX), and part of that Ca^{2+} is taken up by the ER via the sarco-endoplasmic reticulum Ca^{2+}-ATPase (SERCA) (figure 2*a*) [77,80,81]. Analysis of Ca^{2+} dynamics within intracellular stores, ER and mitochondria, simultaneously with $[Ca^{2+}]_i$ in stimulated HeLa cells, revealed that the first $[Ca^{2+}]_i$ oscillation is due to ER Ca^{2+} release with a fraction of that Ca^{2+} taken up by mitochondria, whereas subsequent $[Ca^{2+}]_i$ oscillations are initiated by mitochondrial Ca^{2+} release, which triggers regenerative Ca^{2+} release from the ER [82]. Samanta *et al.* [83] demonstrated that knocking down the MCU significantly inhibits the generation of $[Ca^{2+}]_i$ oscillations in stimulated mast cells, verifying the important role of the MCU in regenerative ER Ca^{2+} release.

During an inflammatory/activated cell state, increases in $[Ca^{2+}]_i$, due to Ca^{2+} release from the ER and/or Ca^{2+} influx from the extracellular space, result in increased $[Ca^{2+}]_m$ which, by stimulating enzymes of the Krebs cycle and oxidative phosphorylation and promoting ATP synthesis, enhances the mitochondrial electron transport chain (ETC) activity/mitochondrial $O_2^{\cdot-}$ production (provided there are no shortages in the supply of O_2 and electron donors [84]) and increases the mROS levels (figure 2*a*) [13,85]. Mitochondrial $O_2^{\cdot-}$ production takes place at ETC complexes I, II and III (mainly I and III; figure 2*a*) [86,87]. Complexes I and II release $O_2^{\cdot-}$ into the matrix, whereas complex III releases $O_2^{\cdot-}$ into both the matrix and the intermembrane space [88]. $O_2^{\cdot-}$ is converted to hydrogen peroxide (H_2O_2) by manganese superoxide dismutase (MnSOD) in the mitochondrial matrix and by copper zinc SOD (CuZnSOD) in the intermembrane space (cytosolic side) [89]. Any H_2O_2 that escapes the mitochondrial antioxidant mechanisms diffuses out and increases the cytosolic ROS levels (especially in the region between ER/mitochondria called mitochondria-associated membranes, MAMs [90]), and can cause oxidative modifications to the IP_3R, SERCA and even the stromal interaction molecule 1 (STIM1)-Orai1 on the plasma membrane, generally resulting in further increase in $[Ca^{2+}]_i$ (due to activation of IP_3R and/or inactivation of SERCA) (figure 2*a*) [13,91–93]. However, the functional consequences of ion channel regulation by the redox state are divergent. For example, a reactive Cys in STIM1 undergoes SSG that promotes Orai1/2 channel opening for Ca^{2+} entry without affecting intracellular store depletion [92], whereas reactive Cys oxidation in Orai1/2 channels inhibits Ca^{2+} entry [94,95]. mROS are involved in a plethora of signalling pathways, such as nuclear factor-κB (NF-κB)- and tumour necrosis factor-α (TNF-α)-induced signalling, leading to expression of cell adhesion molecules and cell dysfunction, but also activation of survival mechanisms [96–102]. ROS were found to exert their effect via SSG of regulatory Cys within NF-κB (inhibited by SSG) and the TNF receptor Fas (activated by SSG) [103–105]. However, the role of SSG of proteins within the mitochondrial compartment in the pathogenesis of cardiovascular disease has not been defined.

Although $[Ca^{2+}]_m$ elevation typically stimulates bioenergetics, under pathological stimuli (endotoxin insult), excessive and persistent $[Ca^{2+}]_m$ elevation causes $[Ca^{2+}]_m$ overload, leading to aberrant electron leak that promotes mROS production and cellular oxidative damage [92,106–108]. Since the mitochondria are one of the main endotoxin-sensitive ROS sources in ECs, it is to be expected that the MCU-mediated mitochondrial Ca^{2+} uptake will be the primary signal for mROS production. $[Ca^{2+}]_m$ and mitochondrial redox balance are generally accepted as both critical and interdependent determinants for EC survival and barrier function [2]. Although $[Ca^{2+}]_m$ and mROS go hand in hand, until recently, it was unknown whether the mROS can oxidatively modify any components of the MCU complex. Our group provided the first evidence that MCU activity is positively modulated via MCU protein oxidation by the luminal mROS [65]. Priming of ECs with endotoxin (oxidative stress) results in thrombin-induced $[Ca^{2+}]_m$ elevation that leads to a further increase in mROS, reduction in ATP production and mitochondrial respiration,

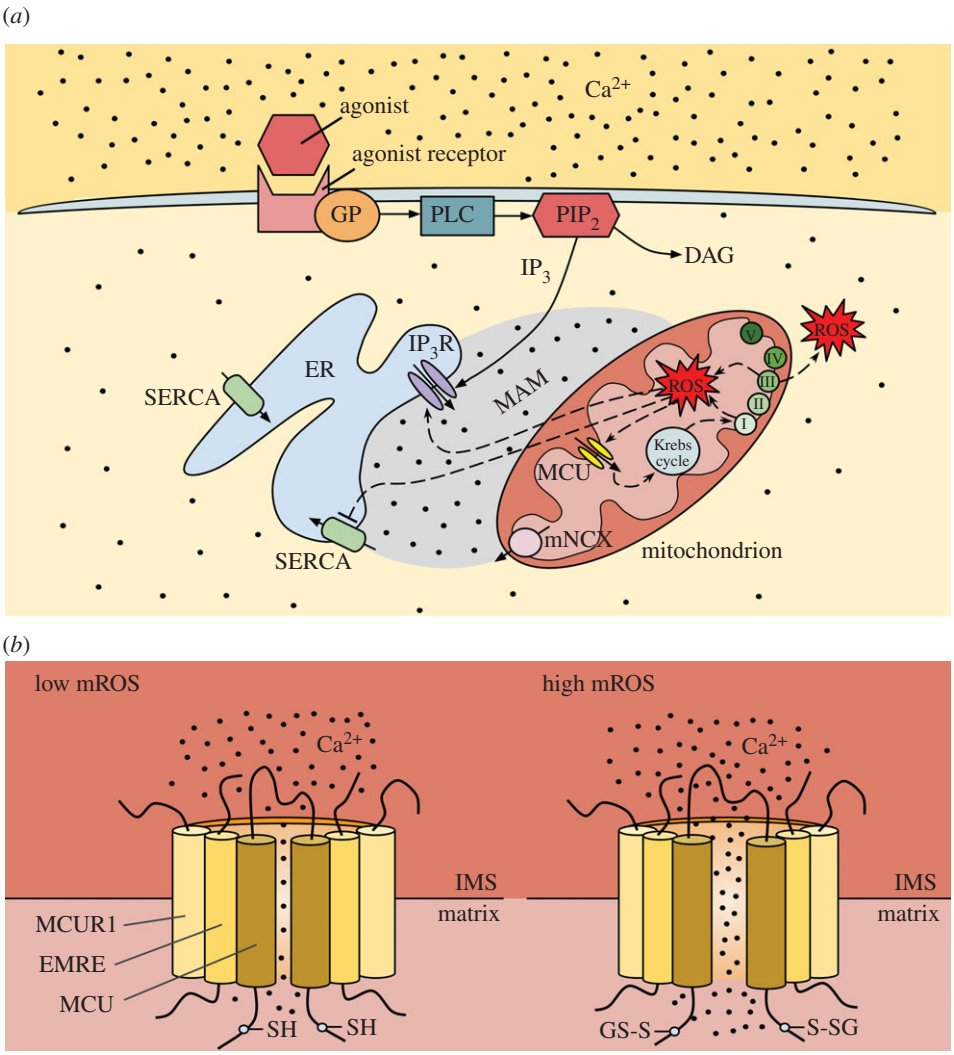

Figure 2. Ca^{2+} and ROS crosstalk between ER and mitochondria, with emphasis on redox control of the MCU. (*a*) In a non-excitable cell exposed to a chemical agonist, binding of the agonist to a cell surface receptor activates the GP/PLC/IP_3 pathway. IP_3 activates the IP_3R and causes Ca^{2+} release from the ER. Both mitochondrial Ca^{2+} uptake via the MCU and Ca^{2+} release via the mNCX differentially regulate the activation of IP_3R in the MAM region (because IP_3R is also regulated by Ca^{2+}) and, thus, play a role in shaping the $[Ca^{2+}]_i$ transients and oscillations in response to the agonist. Mitochondrial Ca^{2+} release is thought to also help refill the ER via the SERCA. High $[Ca^{2+}]_m$ stimulates respiratory chain activity, leading to higher amounts of mROS. MROS can target the MCU and, following diffusion in the MAM region, the IP_3R and SERCA, further amplifying the disruption of Ca^{2+} and ROS homeostasis. (Adapted from [13,75].) (*b*) The MCU senses mROS via oxidation of the matrix-facing Cys-97. S-glutathionylation of Cys-97 induces a conformational change (and causes channel clustering; not shown) leading to increased MCU activity/mitochondrial Ca^{2+} uptake. (Adapted from [65,76].)

upregulation of pro-inflammatory genes, and an increase in apoptosis [65]. mROS appear to only oxidize the core component of the uniporter complex, the MCU itself; other MCU complex components are not susceptible to oxidation under similar conditions [65]. The conserved Cys at position 97 of the human MCU, located in the N-terminal domain of the MCU facing the matrix, is the only reactive thiol within the MCU that undergoes redox modification (SSG) under conditions of high mROS, leading to enhanced MCU activity (figure 2*b*) [65,76]. Although oxidation of the MCU does not alter the interactions of the MCU with its regulators, oxidation induces a conformational change within the N-terminal β-grasp fold, redistributing the MCU complex to form higher order oligomers and increased channel activity. One of the mitochondrial intermembrane space (IMS) proteins, Mia40, both undergoes oxidative folding and mediates protein import to the IMS [109]; however, it is unknown whether it senses mROS. In summary, the MCU has a moonlighting function as a mitochondrial luminal redox sensor that enables mitochondria to decode mROS pathophysiological signals to metabolic or cell death responses. Overall, a better understanding of the Ca^{2+} and ROS crosstalk at the (sub)cellular level is critical, because disruption of mitochondrial Ca^{2+} and mROS (and, as a consequence, of cytosolic Ca^{2+} and ROS) homeostasis has been implicated as the underlying cause in almost every cardiovascular and neurodegenerative disease, as well as in different stages of cancer development [110–113]. It is noteworthy that the interplay between Ca^{2+} and ROS is not limited to the mitochondria. In most pathological conditions, decreases in ER Ca^{2+} levels lead to ER stress/activation of the unfolded protein response (UPR), which, via ER ROS, contributes to the redox regulation of local Ca^{2+} transport [7,13,114].

4. Regulation of mitochondrial Ca^{2+} transport by mechanical forces

Mechanical forces are known factors in regulating every organ system in the human body, but are crucial in the development and physiology of the circulatory system [115,116]. Fluid

mechanical (haemodynamic) forces exerted on the vessel wall are particularly important in vessel structure/remodelling and in vascular pathology, such as atherosclerosis, aneurysms and arteriovenous malformations [117–122]. Atherosclerotic vascular disease continues to be the major cause of death in developed nations [25]. Though influenced by systemic risk factors (hyperlipidaemia, hypertension, diabetes, smoking), atherosclerotic plaques develop preferentially at the outer walls of bifurcations, the inner walls of curvatures and downstream of a stenosis in the carotid, coronary, aortic, renal, iliac, femoral and other arteries [123,124]. It is well accepted that modulation of the vascular EC phenotype by the local haemodynamic forces in those regions contributes to the geometrically focal nature of the disease [26,125–127]. ECs in arteries and arterioles are continuously exposed to three types of haemodynamic stress (force/surface area): normal stress (due to hydrostatic pressure), tensile stress (due to transmural pressure difference) and shear stress (the frictional force exerted by blood flowing over the EC luminal surface) [128,129]. As EC dysfunction is a key and early factor in atherogenesis, and ECs, due to their unique location, experience complex blood flow/shear stress profiles, a lot of research has focused on the effects of shear stress on EC physiology and pathology.

Wall shear stress is the product of blood viscosity and the velocity gradient (slope of the velocity vector in a direction normal to the wall) on the EC luminal surface. For most of the arterial circulation, local wall shear stress can be considered proportional to the volumetric flow rate and inversely proportional to the cube power of the internal radius at each axial position along the blood vessel [130–132]. Using different imaging modalities to measure flow rates and internal diameters, the wall shear stress in straight portions of the arterial vascular network was estimated to vary between 1 and 7 Pa (10–70 dynes cm^{-2}). Those regions, which include locations preceding and following arterial bifurcations as well as the inner walls of flow dividers, are spared from atherosclerotic disease. Flow in those regions is undisturbed (characterized by parallel streamlines), laminar (Reynolds number less than 2100), unsteady (due to the cardiac cycle) and unidirectional; the wall shear stress is called pulsatile (PS) and has a relatively high mean value (figure 3*a*) [119,125,133]. In regions susceptible to disease, such as the outer walls of bifurcations, the local flow is disturbed and reverses during the systole phase of the cardiac cycle (within a flow recirculation zone with high temporal and spatial shear stress gradients), but it is still laminar; the wall shear stress is called oscillatory (OS), has a mean close to zero and varies between ± 0.6 Pa (6 dynes cm^{-2}) (figure 3*a*) [119,125,133]. Histology and digital image analysis of microparticle flow in post-mortem arteries, non-invasive (magnetic resonance phase velocity mapping) and invasive imaging modalities (coronary angiography, intravascular ultrasound), together with computational fluid dynamics, have verified the spatial correlation between OS and atherosclerosis initiation and progression in animals and humans [120,124,134,135].

In order to understand the EC phenotypes due to exposure to different shear stress profiles, many groups have subjected cultured ECs from different species and vascular beds (or *ex vivo* arteries) to controlled flow conditions using perfusion chambers/systems or cone-and-plate viscometers followed by biochemical analysis at both the gene and protein levels [126,136–140]. With few exceptions, most of those studies approximated PS and OS profiles as sinusoidal waves of fixed amplitude and period (figure 3*b*). For corresponding controls, cultured ECs were either exposed to undisturbed laminar steady shear stress (SS) at a value equal to the PS time-average or were left static (figure 3*b*). For verification of findings *in vivo*, the endothelium was isolated from regions in animal arteries known to be exposed to either PS or OS, and analysed for differential gene expression (mRNA, miRNA), and these databases drove further *in vitro* experimentation on upstream intracellular signalling pathways and downstream cell behaviour [127,141,142]. Changing arterial flow in animals by creating a stenosis through partial ligation (OS develops downstream) established the causal relationship between OS and atherogenesis [143]. *In vitro* studies showed the existence of metrics of PS and OS, besides the main ones (mean value, amplitude and period), such as shear stress angular direction, harmonic frequencies and oscillatory shear index, that are also sensed by ECs [144–146]; in this review, we will refer to PS and OS based solely on their main metrics. Overall, both *in vivo* and *in vitro* studies verified that OS induces EC inflammation and dysfunction, which, in the presence of additional systemic risk factors, primes the OS-exposed arterial regions for disease initiation. It is noteworthy that the detrimental effect of OS is not purely mechanical; prolonged residence time of cytokines and other chemicals released by ECs and trapped blood cells in the flow recirculation zone contributes to the EC dysfunction.

PS (or SS) is known to decrease the EC proliferation rate and extent of apoptosis (the latter, following EC exposure to a stimulus that causes oxidative stress), rendering the endothelium 'atheroresistant', whereas OS does the opposite ('atherosusceptible' endothelium) [147–150]. The atheroprotective effect of PS (or SS) is, to a large extent, due to shear-induced expression and activation of endothelial nitric oxide synthase (eNOS) that produces the vasodilator NO (figure 3*c*) [151–154]. By contrast, eNOS expression was decreased under OS *in vivo*, compared with PS, and *in vitro*, compared with static controls (figure 3*d*) [153,155,156]. In agreement with that, isolated arterioles from animals/humans showed NO-dependent dilation under PS or SS; OS did not induce dilation [157,158]. PS (or SS) was found to trigger EC secretion of ATP causing autocrine/paracrine activation of surface purinergic receptors (G_q/G_{11} protein-coupled $P2Y_2$Rs), activation of PLC, generation of IP_3, release of Ca^{2+} from the ER IP_3R, and $[Ca^{2+}]_i$ transients, which led to sequential phosphorylation of platelet/endothelial cell adhesion molecule-1 (PECAM-1), vascular endothelial growth factor receptor 2 (VEGFR2), Akt and eNOS [159–161]. $[Ca^{2+}]_i$ signalling is necessary for eNOS activation, because $P2Y_2$R deficiency blocked both the shear-induced $[Ca^{2+}]_i$ transients and PECAM-1/VEGFR2/Akt/eNOS activation [161]. $[Ca^{2+}]_i$ signalling is also important for PS (or SS)-induced eNOS expression, which occurs due to Ca^{2+}/CaM-mediated phosphorylation/nuclear export of histone deacetylase 5 (HDAC5) and resultant expression of Krüppel-like factors 2 and 4 (KLF2/4), both of which are transcription factors for eNOS [162]. eNOS is transcriptionally repressed under OS due to miR-92a targeting of KLF2/4 [156,163] and probably also due to increased expression/activation of the tumour suppressor p53 [164,165].

Several groups measured SS-induced EC $[Ca^{2+}]_i$ changes, but reported conflicting data regarding the type of the response (single transient versus oscillations) and the relative contribution of Ca^{2+} release from the ER versus Ca^{2+} entry from the extracellular space [166–172]. Most of them spatially

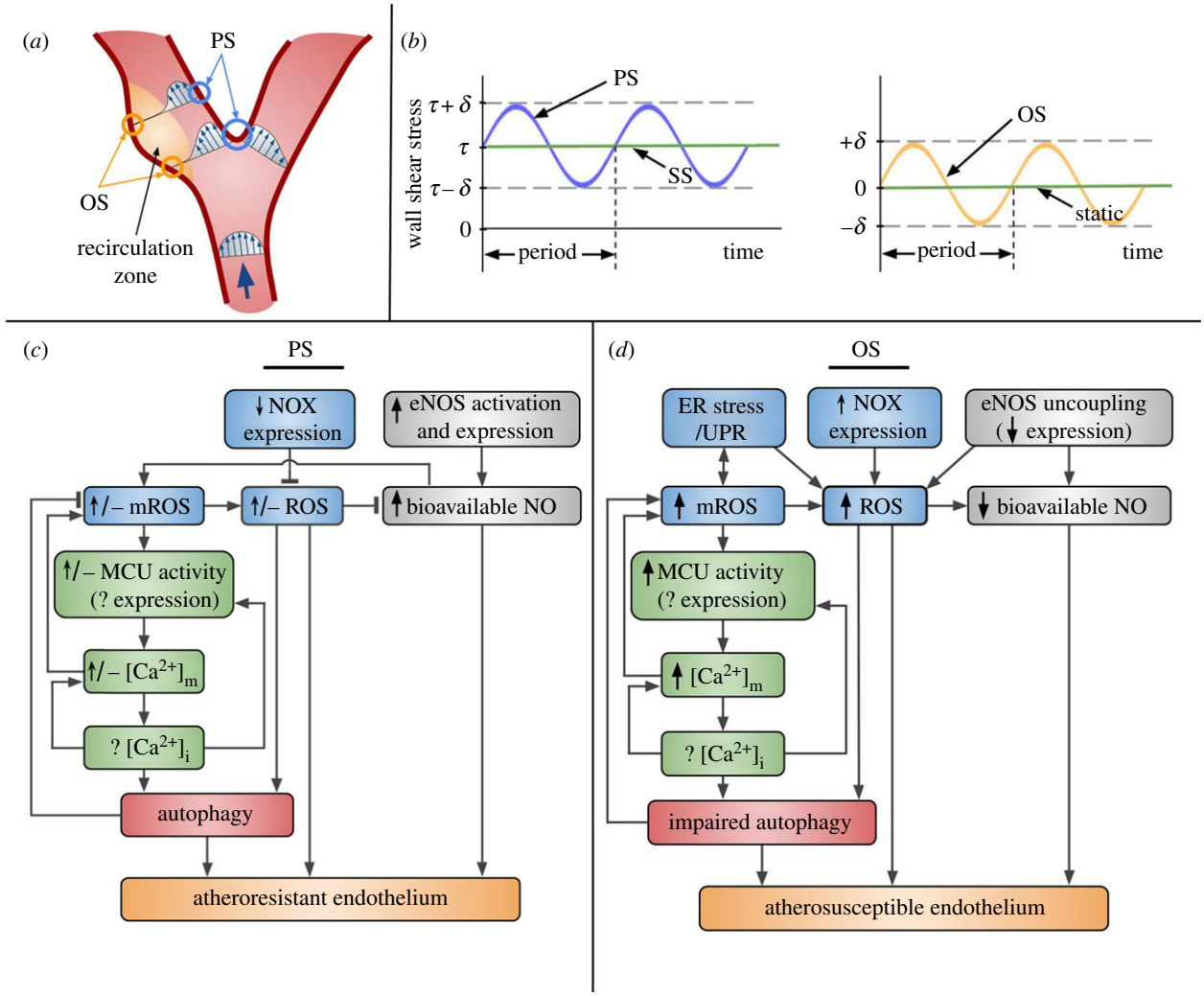

Figure 3. Fluid shear stress profiles and their effects on Ca^{2+} and ROS signalling in the vascular endothelium. (*a*) Schematic of axial velocity profiles at different locations in a vascular bifurcation, such as the carotid, coronary, renal and iliac artery flow dividers. (Adapted from [119].) Regions on the vessel wall exposed to PS (blue circles) are spared from atherosclerotic disease, whereas those in the flow recirculation zone (yellow circles) are exposed to OS and are prone to disease. (*b*) Idealized shear stress profiles versus time are shown for PS, SS, OS and static controls (used in *in vitro* studies). (*c*) PS onset raises cytosolic ROS levels; both cytosolic ROS and mROS levels decline/return to baseline at longer times. ROS levels decline due to decreased NOX expression, but any remaining $O_2^{\cdot-}$/ROS scavenge NO. NO levels are high due to increased eNOS activation and, at longer times, expression. NO promotes generation of mitochondrial $O_2^{\cdot-}$/mROS. MROS regulate the MCU activity (shear-induced changes in expression of the MCU and its regulators are currently unknown) and, via $[Ca^{2+}]_m$, are expected to affect the $[Ca^{2+}]_i$ response (and vice versa). $[Ca^{2+}]_i$ drives MCU expression. $[Ca^{2+}]_m$ increases mitochondrial $O_2^{\cdot-}$/mROS. $[Ca^{2+}]_i$ and mROS/cytosolic ROS are known to regulate autophagy, which is reported to be fully functional under PS, and, thus, helps maintain mROS levels under control. The combination of high bioavailable NO, low ROS and functional autophagy results in the atheroresistant endothelial phenotype. (*d*) Under OS, ER stress/UPR contributes to increased mROS (and vice versa) and cytosolic ROS levels. Upregulated NOXs also lead to increased cytosolic ROS levels. eNOS uncoupling further contributes ROS. Increased cytosolic ROS and downregulated eNOS expression result in decreased NO levels. Elevated mROS levels enhance the MCU activity (any changes in mRNA/protein levels are unknown), which leads to increased $[Ca^{2+}]_m$ with unknown, but anticipated, effects on $[Ca^{2+}]_i$. Autophagy, under regulation by $[Ca^{2+}]_i$ and mROS/cytosolic ROS, is impaired (specifically, the flux is impaired) under OS. The combination of diminished NO, high ROS, and dysfunctional autophagy results in the atherosusceptible endothelial phenotype.

averaged fluorescence signals from Ca^{2+}-sensitive probes over ECs in a microscope field of view and reported an initial peak followed by a slow decline to baseline in response to SS. By monitoring $[Ca^{2+}]_i$ changes versus time in individual cells, our group concluded that a significant percentage of ECs respond to SS with $[Ca^{2+}]_i$ oscillations (repetitive transients), and $[Ca^{2+}]_i$ peak amplitudes and oscillation frequencies depend on the SS level [75]. Importantly, the SS-induced $[Ca^{2+}]_i$ response was due to release of Ca^{2+} from the ER and required $[Ca^{2+}]_m$ uptake via the MCU and release via the mNCX [75]. As Ca^{2+} is known to regulate the IP_3R in a biphasic manner (§3), these data suggested that mitochondrial Ca^{2+} uptake via the MCU within the MAMs may suppress the Ca^{2+}-inhibitory effect on IP_3R (following prior ER Ca^{2+} release), causing continuation of ER Ca^{2+} release and recurrence of $[Ca^{2+}]_i$ oscillations [75]. Not only is $[Ca^{2+}]_i$ regulated by mitochondrial Ca^{2+} transport, but also $[Ca^{2+}]_m$ is controlled by $[Ca^{2+}]_i$ via Ca^{2+}-mediated activation of CREB, the transcription factor that induces MCU expression [173]. A group that measured $[Ca^{2+}]_i$ under PS versus OS reported $[Ca^{2+}]_i$ oscillations in ECs exposed to either flow, an initial peak in spatially averaged $[Ca^{2+}]_i$ in PS-exposed ECs, and maintenance of spatially averaged $[Ca^{2+}]_i$ at baseline in OS-exposed ECs [174,175]. Prendergast *et al.* [176] showed enhanced $[Ca^{2+}]_i$ signals in ECs from thoracic aorta (PS-exposed) compared with ECs from aortic arch (OS-exposed) in isolated tissues from either wild-type (WT) or $ApoE^{-/-}$ mice (prior to lesion development) following exposure to

carbachol, suggesting that $[Ca^{2+}]_i$ responses in OS-conditioned ECs may be blunted compared with those in PS-conditioned ECs. This agrees with recent findings by Taylor *et al.* [177], who showed that acetylcholine (ACh)-induced EC $[Ca^{2+}]_i$ dynamics were diminished in carotid arterial regions proximal to a partial ligation (OS-exposed), compared with PS-exposed control regions, in WT mice. To the best of our knowledge, the role of mitochondrial Ca^{2+} transport in $[Ca^{2+}]_i$ has not been examined in ECs under the physiological flow profiles PS and OS. Concurrent recordings of spatio-temporal profiles of $[Ca^{2+}]_i$ and $[Ca^{2+}]_m$ have shed light on the communication between the two Ca^{2+} pools in different cell types under chemical stimulation [5,82,83,178,179], but these experiments have not been conducted in ECs exposed to shear stress. Interestingly, work by the Pozzan group showed that MCU overexpression, via enhanced Ca^{2+} buffering by mitochondria, reduces the $[Ca^{2+}]_i$ peaks both during spontaneous oscillations and following caffeine treatment in cardiomyocytes [180]. A higher EC MCU activity (and/or expression) in OS- versus PS-exposed arterial regions would lead to increased mitochondrial Ca^{2+} uptake and would explain the reported diminished $[Ca^{2+}]_i$ responses under OS.

The pro-inflammatory signalling pathways underlying atherogenesis, including c-Jun N-terminal kinase (JNK)/the family of mitogen-activated protein kinases (MAPKs) and the transcription factors NF-κB and activator protein-1 (AP-1), are redox sensitive [181]. OS was found to cause a sustained increase in $O_2^{\cdot-}$ production/ROS levels, whereas PS (or SS) induced an increase upon the onset of flow, but, after the first couple of hours, the increase in ROS was compensated by upregulation of antioxidant defences, such as haem oxygenase-1 (HO-1) and NADPH quinone oxidoreductase 1 (NQO1), under the control of nuclear factor erythroid 2-related factor 2 (Nrf2) [153,182–186]. NADPH oxidases (NOXs), xanthine oxidase, mitochondria and uncoupled eNOS are the main sources of cytosolic ROS in ECs [187]. PS (or SS) downregulated NOX4 expression; OS upregulated NOX1 and NOX2 expression in parallel with xanthine oxidase levels, with mixed results regarding the OS effects on NOX4 (figure 3*c*,*d*) [153,188]. NOX1-derived ROS, in particular, were responsible for activation of NF-κB and upregulation of intercellular adhesion molecule-1 (ICAM-1) in OS-exposed ECs *in vitro* and *in vivo* [188]. Shear-induced ROS are expected to play a key role in Ca^{2+} homeostasis, because the second messengers are known to interact in a bidirectional manner (in general, increased $[Ca^{2+}]_i$ causes an increase in $[Ca^{2+}]_m$ and mROS, whereas increased mROS result in a further increase in $[Ca^{2+}]_m$) (figure 3*c*,*d*). In addition, ECs in atheroprone areas *in vivo* were found to undergo ER stress, and UPR activation is associated with increased ER ROS [114,127,189]. Increased mROS are thought to both activate ER stress/UPR and be the result of ER stress/UPR (the latter due to increased Ca^{2+} release from the ER resulting in elevated $[Ca^{2+}]_i$ and $[Ca^{2+}]_m$) (figure 3*c*,*d*) [13,190]. Any $O_2^{\cdot-}$ in the cytosol/organelles that escaped antioxidant defences is consumed by a diffusion-limited reaction with NO to form the reactive nitrogen species (RNS) peroxynitrite ($ONOO^-$), thus lowering the bioavailable NO levels ($ONOO^-$ can also uncouple eNOS) and promoting atherosclerosis [191,192]. Either OS-exposed ECs *in vitro* or atheroprone regions *in vivo* had increased levels of nitrotyrosine, the footprint of $ONOO^-$ formation, compared with PS-exposed ECs and atheroresistant regions, respectively (due to increased $O_2^{\cdot-}$ production and despite decreased NO generation under OS) [193]. Even following short exposure of cultured ECs to SS, low levels of $ONOO^-$ formed in mitochondria resulted in partial inhibition of mitochondrial respiratory complexes and increased mitochondrial $O_2^{\cdot-}$/ROS levels; the effect was attenuated when SS was performed at lower than atmospheric (closer to arterial) O_2 levels [194,195]. Interestingly, NOX-derived $O_2^{\cdot-}$/ROS were found to either activate or inactivate eNOS: under SS (and one might assume the same for PS), activated NOX2/p47phox and resultant ROS were responsible for eNOS activation, whereas, under OS, ROS from activated NOX1/NOXO1 caused eNOS uncoupling leading to eNOS-derived $O_2^{\cdot-}$/ROS and a concomitant decrease in NO production/bioavailable levels (figure 3*c*,*d*) [196]. Based on the higher levels of mROS/cytosolic ROS in OS-exposed ECs compared with PS (or SS)-exposed ECs and the recently discovered mROS sensing by the MCU [65], one can speculate that there may be increased MCU activity/mitochondrial Ca^{2+} uptake/$[Ca^{2+}]_m$ levels under OS versus PS (figure 3*c*,*d*), which may be the reason behind the OS-induced EC inflammation and decreased cell resistance to apoptosis.

5. Mitochondrial Ca^{2+} uniporter: a potential therapeutic target in vascular diseases

The speculation regarding altered MCU activity in the endothelium of atheroprone regions, compared with activation in atheroprotective ones, is in agreement with the oxidative stress and inflammation encountered in those locations. Specifically, under OS, increased $[Ca^{2+}]_m$/mROS/cytosolic ROS would dampen NO bioavailability and render the endothelium dysfunctional, which could result in vascular risk factors (figure 3*d*). It is safe to assume that, even if the global EC $[Ca^{2+}]_i$ does not change significantly in OS-exposed regions, $[Ca^{2+}]_i$ in specific locations of the cytosol, such as in proximity to the mitochondria (e.g. the MAMs), could influence $[Ca^{2+}]_m$ overload. Based on the speculation of regional dependency of MCU activity, graded inhibition of MCU activity (and/or expression), down to levels encountered in atheroprotective regions, may be a great strategy to prevent EC dysfunction and atherosclerotic disease initiation/progression. As MCU activity is elevated following its oxidative modification by mROS [65], administration of mitochondria-targeted antioxidants would have a beneficial effect. In agreement with this notion, Li *et al.* [197] showed that human aortic ECs (HAECs) treated with the pro-inflammatory lipid lysophosphatidylcholine increased their mROS due to enhanced MCU activation; both were attenuated in the presence of the mROS scavenger mitoTEMPO. MitoTEMPO also suppressed EC activation and monocyte recruitment in the aorta of $ApoE^{-/-}$ mice fed with a high-fat diet [197]. Although this study did not examine specific aortic locations, the beneficial effect of the drug would be apparent in locations that experience OS. Decreasing mitochondrial Ca^{2+} entry *in vitro* can also be done by knocking down proteins involved in ER–mitochondria contact sites and, thus, increasing the MAM width. Although this method cannot be translated to clinical settings, nevertheless it was shown that it protects cultured cells from oxidative stress-induced apoptosis [198]. One of the reasons why graded inhibition of MCU activity may be able to maintain EC health in OS-exposed regions is its potential impact on autophagy. Autophagy is a critical homeostatic mechanism in

cardiovascular health [199–201]. Functional autophagy was shown to be a prerequisite for the SS-induced increase in NO production [202,203]. Dysfunctional autophagy occurs when autophagy induction (autophagosome formation) becomes highly activated and, as a result, the autophagic flux (rate of autophagosome–lysosome fusion and degradation of autophagosomal cargo) slows down ('impaired' flux) leading to inadequate removal of dysfunctional mitochondria and a tonic increase in oxidative stress. Li *et al.* [204] showed that OS exposure increases the induction of autophagy, but decreases the autophagic flux in cultured HAECs (whereas PS maintains autophagy at levels comparable to static controls); both the increased induction and decreased flux under OS were mediated by JNK activation and elevated mROS. The impaired EC autophagic flux was verified in OS-exposed regions of rabbit aortas [204]. Graded inhibition of MCU activation in OS-exposed regions will reduce mROS, which, by lowering autophagy induction, should allow for, at least, partial normalization of the impaired flux, in agreement with a recent review [205]. In support of the importance of a functional autophagic flux in EC health, it was recently shown that SS upregulates the transcription factor EB (TFEB), master regulator of autophagic flux and lysosomal biogenesis, and that transgenic mice with EC-specific TFEB expression exhibit reduced leucocyte recruitment to ECs and decreased development of atherosclerosis [206]. Since mitochondrial ion homeostasis plays a major role in endothelial function, we put forward a hypothesis that perturbation of mitochondrial Ca^{2+} homeostasis could lead to several vascular pathological conditions.

Data accessibility. This article has no additional data.

Authors' contributions. B.R.A. and M.M. conceived the themes of this manuscript. B.R.A., S.S., A.P., P.B.S. and M.M. drafted the manuscript. All authors gave final approval for publication.

Competing interests. We declare we have no competing interests.

Funding. B.R.A. is supported by an American Heart Association Grant-in-Aid. P.B.S. is supported by the Natural Sciences and Engineering Research Council of Canada, Prostate Cancer Canada Network (Telus Ride for Dad) and the Canadian Foundation for Innovation. M.M. is supported by NIH R01GM109882, R01HL086699, R01HL119306 and 1S10RR027327 grants.

Acknowledgement. The authors wish to thank Dr Peter F. Davies, University of Pennsylvania, for a critical review and thoughtful comments.

References

1. Sandow SL, Senadheera S, Grayson TH, Welsh DG, Murphy TV. 2012 Calcium and endothelium-mediated vasodilator signaling. *Adv. Exp. Med. Biol.* **740**, 811–831. (doi:10.1007/978-94-007-2888-2_36)
2. Widlansky ME, Gutterman DD. 2011 Regulation of endothelial function by mitochondrial reactive oxygen species. *Antioxid. Redox Signal.* **15**, 1517–1530. (doi:10.1089/ars.2010.3642)
3. Godo S, Shimokawa H. 2017 Endothelial functions. *Arterioscler. Thromb. Vasc. Biol.* **37**, e108–e114. (doi:10.1161/ATVBAHA.117.309813)
4. Cobbold PH, Cuthbertson KS. 1990 Calcium oscillations: phenomena, mechanisms and significance. *Semin. Cell. Biol.* **1**, 311–321.
5. Hajnoczky G, Robb-Gaspers LD, Seitz MB, Thomas AP. 1995 Decoding of cytosolic calcium oscillations in the mitochondria. *Cell* **82**, 415–424. (doi:10.1016/0092-8674(95)90430-1)
6. Bravo-Sagua R, Parra V, Lopez-Crisosto C, Diaz P, Quest AF, Lavandero S. 2017 Calcium transport and signaling in mitochondria. *Compr. Physiol.* **7**, 623–634. (doi:10.1002/cphy.c160013)
7. Raffaello A, Mammucari C, Gherardi G, Rizzuto R. 2016 Calcium at the center of cell signaling: interplay between endoplasmic reticulum, mitochondria, and lysosomes. *Trends Biochem. Sci.* **41**, 1035–1049. (doi:10.1016/j.tibs.2016.09.001)
8. Pinton P, Pozzan T, Rizzuto R. 1998 The Golgi apparatus is an inositol 1,4,5-trisphosphate-sensitive Ca^{2+} store, with functional properties distinct from those of the endoplasmic reticulum. *EMBO J.* **17**, 5298–5308. (doi:10.1093/emboj/17.18.5298)
9. Calcraft PJ *et al.* 2009 NAADP mobilizes calcium from acidic organelles through two-pore channels. *Nature* **459**, 596–600. (doi:10.1038/nature08030)
10. Caja S, Enriquez JA. 2017 Mitochondria in endothelial cells: sensors and integrators of environmental cues. *Redox Biol.* **12**, 821–827. (doi:10.1016/j.redox.2017.04.021)
11. Kluge MA, Fetterman JL, Vita JA. 2013 Mitochondria and endothelial function. *Circ. Res.* **112**, 1171–1188. (doi:10.1161/CIRCRESAHA.111.300233)
12. Scheitlin CG, Nair DM, Crestanello JA, Zweier JL, Alevriadou BR. 2014 Fluid mechanical forces and endothelial mitochondria: a bioengineering perspective. *Cell. Mol. Bioeng.* **7**, 483–496. (doi:10.1007/s12195-014-0357-4)
13. Gorlach A, Bertram K, Hudecova S, Krizanova O. 2015 Calcium and ROS: a mutual interplay. *Redox Biol.* **6**, 260–271. (doi:10.1016/j.redox.2015.08.010)
14. Baughman JM *et al.* 2011 Integrative genomics identifies MCU as an essential component of the mitochondrial calcium uniporter. *Nature* **476**, 341–345. (doi:10.1038/nature10234)
15. De Stefani D, Raffaello A, Teardo E, Szabo I, Rizzuto R. 2011 A forty-kilodalton protein of the inner membrane is the mitochondrial calcium uniporter. *Nature* **476**, 336–340. (doi:10.1038/nature10230)
16. Tomar D *et al.* 2016 MCUR1 is a scaffold factor for the MCU complex function and promotes mitochondrial bioenergetics. *Cell Rep.* **15**, 1673–1685. (doi:10.1016/j.celrep.2016.04.050)
17. Antony AN *et al.* 2016 MICU1 regulation of mitochondrial Ca^{2+} uptake dictates survival and tissue regeneration. *Nat. Commun.* **7**, 10955. (doi:10.1038/ncomms10955)
18. Patron M *et al.* 2014 MICU1 and MICU2 finely tune the mitochondrial Ca^{2+} uniporter by exerting opposite effects on MCU activity. *Mol. Cell* **53**, 726–737. (doi:10.1016/j.molcel.2014.01.013)
19. Sancak Y *et al.* 2013 EMRE is an essential component of the mitochondrial calcium uniporter complex. *Science* **342**, 1379–1382. (doi:10.1126/science.1242993)
20. Raffaello A *et al.* 2013 The mitochondrial calcium uniporter is a multimer that can include a dominant-negative pore-forming subunit. *EMBO J.* **32**, 2362–2376. (doi:10.1038/emboj.2013.157)
21. Hoffman NE *et al.* 2013 MICU1 motifs define mitochondrial calcium uniporter binding and activity. *Cell Rep.* **5**, 1576–1588. (doi:10.1016/j.celrep.2013.11.026)
22. Mallilankaraman K *et al.* 2012 MICU1 is an essential gatekeeper for MCU-mediated mitochondrial Ca^{2+} uptake that regulates cell survival. *Cell* **151**, 630–644. (doi:10.1016/j.cell.2012.10.011)
23. Mallilankaraman K *et al.* 2012 MCUR1 is an essential component of mitochondrial Ca^{2+} uptake that regulates cellular metabolism. *Nat. Cell Biol.* **14**, 1336–1343. (doi:10.1038/ncb2622)
24. Perocchi F, Gohil VM, Girgis HS, Bao XR, McCombs JE, Palmer AE, Mootha VK. 2010 MICU1 encodes a mitochondrial EF hand protein required for Ca^{2+} uptake. *Nature* **467**, 291–296. (doi:10.1038/nature09358)
25. Mozaffarian D 2016 Heart disease and stroke statistics—2016 update: a report from the American Heart Association. *Circulation* **133**, e38–360. (doi:10.1161/CIR.0000000000000350)
26. Gimbrone Jr MA, Garcia-Cardena G. 2016 Endothelial cell dysfunction and the pathobiology of atherosclerosis. *Circ. Res.* **118**, 620–636. (doi:10.1161/CIRCRESAHA.115.306301)
27. Nigro P, Abe J, Berk BC. 2011 Flow shear stress and atherosclerosis: a matter of site specificity. *Antioxid. Redox Signal.* **15**, 1405–1414. (doi:10.1089/ars.2010.3679)
28. Martell JD, Deerinck TJ, Sancak Y, Poulos TL, Mootha VK, Sosinsky GE, Ellisman MH, Ting AY. 2012 Engineered ascorbate peroxidase as a genetically

encoded reporter for electron microscopy. *Nat. Biotechnol.* **30**, 1143–1148. (doi:10.1038/nbt.2375)

29. Ahuja M, Muallem S. 2014 The gatekeepers of mitochondrial calcium influx: MICU1 and MICU2. *EMBO Rep.* **15**, 205–206. (doi:10.1002/embr.201438446)
30. Csordas G *et al.* 2013 MICU1 controls both the threshold and cooperative activation of the mitochondrial Ca^{2+} uniporter. *Cell Metab.* **17**, 976–987. (doi:10.1016/j.cmet.2013.04.020)
31. Kamer KJ, Mootha VK. 2014 MICU1 and MICU2 play nonredundant roles in the regulation of the mitochondrial calcium uniporter. *EMBO Rep.* **15**, 299–307. (doi:10.1002/embr.201337946)
32. Foskett JK, Madesh M. 2014 Regulation of the mitochondrial Ca^{2+} uniporter by MICU1 and MICU2. *Biochem. Biophys. Res. Commun.* **449**, 377–383. (doi:10.1016/j.bbrc.2014.04.146)
33. Liu JC *et al.* 2016 MICU1 serves as a molecular gatekeeper to prevent *in vivo* mitochondrial calcium overload. *Cell Rep.* **16**, 1561–1573. (doi:10.1016/j.celrep.2016.07.011)
34. Hoffman NE *et al.* 2014 SLC25A23 augments mitochondrial Ca^{2+} uptake, interacts with MCU, and induces oxidative stress-mediated cell death. *Mol. Biol. Cell* **25**, 936–947. (doi:10.1091/mbc.E13-08-0502)
35. Igbavboa U, Pfeiffer DR. 1988 EGTA inhibits reverse uniport-dependent Ca^{2+} release from uncoupled mitochondria. Possible regulation of the Ca^{2+} uniporter by a Ca^{2+} binding site on the cytoplasmic side of the inner membrane. *J. Biol. Chem.* **263**, 1405–1412.
36. Kamer KJ, Grabarek Z, Mootha VK. 2017 High-affinity cooperative Ca^{2+} binding by MICU1-MICU2 serves as an on-off switch for the uniporter. *EMBO Rep.* **18**, 1397–1411. (doi:10.15252/embr.201643748)
37. Kroner H. 1986 Ca^{2+} ions, an allosteric activator of calcium uptake in rat liver mitochondria. *Arch. Biochem. Biophys.* **251**, 525–535. (doi:10.1016/0003-9861(86)90360-7)
38. Moreau B, Nelson C, Parekh AB. 2006 Biphasic regulation of mitochondrial Ca^{2+} uptake by cytosolic Ca^{2+} concentration. *Curr. Biol.* **16**, 1672–1677. (doi:10.1016/j.cub.2006.06.059)
39. Plovanich M *et al.* 2013 MICU2, a paralog of MICU1, resides within the mitochondrial uniporter complex to regulate calcium handling. *PLoS ONE* **8**, e55785. (doi:10.1371/journal.pone.0055785)
40. Lam SS, Martell JD, Kamer KJ, Deerinck TJ, Ellisman MH, Mootha VK, Ting AY. 2015 Directed evolution of APEX2 for electron microscopy and proximity labeling. *Nat. Methods* **12**, 51–54. (doi:10.1038/nmeth.3179)
41. Holm L, Rosenstrom P. 2010 Dali server: conservation mapping in 3D. *Nucleic Acids Res.* **38**(Web Server issue):W545–W549. (doi:10.1093/nar/gkq366)
42. Holm L, Kaariainen S, Rosenstrom P, Schenkel A. 2008 Searching protein structure databases with DaliLite v.3. *Bioinformatics* **24**, 2780–2781. (doi:10.1093/bioinformatics/btn507)
43. Wang L, Yang X, Li S, Wang Z, Liu Y, Feng J, Zhu Y, Shen Y. 2014 Structural and mechanistic insights into MICU1 regulation of mitochondrial calcium uptake. *EMBO J.* **33**, 594–604. (doi:10.1002/embj.201386523)
44. Bhattacharya S, Bunick CG, Chazin WJ. 2004 Target selectivity in EF-hand calcium binding proteins. *Biochim. Biophys. Acta* **1742**, 69–79. (doi:10.1016/j.bbamcr.2004.09.002)
45. Chazin WJ. 2011 Relating form and function of EF-hand calcium binding proteins. *Acc. Chem. Res.* **44**, 171–179. (doi:10.1021/ar100110d)
46. Hoeflich KP, Ikura M. 2002 Calmodulin in action: diversity in target recognition and activation mechanisms. *Cell* **108**, 739–742. (doi:10.1016/S0092-8674(02)00682-7)
47. Kawasaki H, Kretsinger RH. 2014 Structural differences among subfamilies of EF-hand proteins—a view from the pseudo two-fold symmetry axis. *Proteins* **82**, 2915–2924. (doi:10.1002/prot.24562)
48. Stathopulos PB, Ikura M. 2013 Structure and function of endoplasmic reticulum STIM calcium sensors. *Curr. Top. Membr.* **71**, 59–93. (doi:10.1016/B978-0-12-407870-3.00003-2)
49. Bezprozvanny I, Watras J, Ehrlich BE. 1991 Bell-shaped calcium-response curves of $Ins(1,4,5)P_3$- and calcium-gated channels from endoplasmic reticulum of cerebellum. *Nature* **351**, 751–754. (doi:10.1038/351751a0)
50. Mak DO, McBride S, Foskett JK. 1998 Inositol 1,4,5-tris-phosphate activation of inositol tris-phosphate receptor Ca^{2+} channel by ligand tuning of Ca^{2+} inhibition. *Proc. Natl Acad. Sci. USA* **95**, 15 821–15 825. (doi:10.1073/pnas.95.26.15821)
51. Meissner G, Darling E, Eveleth J. 1986 Kinetics of rapid Ca^{2+} release by sarcoplasmic reticulum. Effects of Ca^{2+}, Mg^{2+}, and adenine nucleotides. *Biochemistry* **25**, 236–244. (doi:10.1021/bi00349a033)
52. Hoth M, Penner R. 1993 Calcium release-activated calcium current in rat mast cells. *J. Physiol.* **465**, 359–386. (doi:10.1113/jphysiol.1993.sp019681)
53. Zweifach A, Lewis RS. 1995 Rapid inactivation of depletion-activated calcium current (ICRAC) due to local calcium feedback. *J. Gen. Physiol.* **105**, 209–226. (doi:10.1085/jgp.105.2.209)
54. Kirichok Y, Krapivinsky G, Clapham DE. 2004 The mitochondrial calcium uniporter is a highly selective ion channel. *Nature* **427**, 360–364. (doi:10.1038/nature02246)
55. Collins TJ, Lipp P, Berridge MJ, Bootman MD. 2001 Mitochondrial Ca^{2+} uptake depends on the spatial and temporal profile of cytosolic Ca^{2+} signals. *J. Biol. Chem.* **276**, 26 411–26 420. (doi:10.1074/jbc.M101101200)
56. Maechler P, Kennedy ED, Wang H, Wollheim CB. 1998 Desensitization of mitochondrial Ca^{2+} and insulin secretion responses in the beta cell. *J. Biol. Chem.* **273**, 20 770–20 778. (doi:10.1074/jbc.273.33.20770)
57. Moreau B, Parekh AB. 2008 Ca^{2+}-dependent inactivation of the mitochondrial Ca^{2+} uniporter involves proton flux through the ATP synthase. *Curr. Biol.* **18**, 855–859. (doi:10.1016/j.cub.2008.05.026)
58. Pinton P, Leo S, Wieckowski MR, Di Benedetto G, Rizzuto R. 2004 Long-term modulation of mitochondrial Ca^{2+} signals by protein kinase C isozymes. *J. Cell Biol.* **165**, 223–232. (doi:10.1083/jcb.200311061)
59. Vais H, Mallilankaraman K, Mak DO, Hoff H, Payne R, Tanis JE, Foskett JK. 2016 EMRE is a matrix Ca^{2+} sensor that governs gatekeeping of the mitochondrial Ca^{2+} uniporter. *Cell Rep.* **14**, 403–410. (doi:10.1016/j.celrep.2015.12.054)
60. Tsai MF, Phillips CB, Ranaghan M, Tsai CW, Wu Y, Willliams C, Miller C. 2016 Dual functions of a small regulatory subunit in the mitochondrial calcium uniporter complex. *eLife* **5**, e15545. (doi:10.7554/eLife.15545).
61. Yamamoto T *et al.* 2016 Analysis of the structure and function of EMRE in a yeast expression system. *Biochim. Biophys. Acta* **1857**, 831–839. (doi:10.1016/j.bbabio.2016.03.019)
62. Oxenoid K *et al.* 2016 Architecture of the mitochondrial calcium uniporter. *Nature* **533**, 269–273. (doi:10.1038/nature17656)
63. Cao C, Wang S, Cui T, Su XC, Chou JJ. 2017 Ion and inhibitor binding of the double-ring ion selectivity filter of the mitochondrial calcium uniporter. *Proc. Natl Acad. Sci. USA* **114**, E2846–E2851. (doi:10.1073/pnas.1620316114)
64. Lee SK *et al.* 2016 Structural insights into mitochondrial calcium uniporter regulation by divalent cations. *Cell Chem. Biol.* **23**, 1157–1169. (doi:10.1016/j.chembiol.2016.07.012)
65. Dong Z *et al.* 2017 Mitochondrial Ca^{2+} uniporter is a mitochondrial luminal redox sensor that augments MCU channel activity. *Mol. Cell* **65**, 1014–1028.e7. (doi:10.1016/j.molcel.2017.01.032)
66. Lee Y *et al.* 2015 Structure and function of the N-terminal domain of the human mitochondrial calcium uniporter. *EMBO Rep.* **16**, 1318–1333. (doi:10.15252/embr.201540436)
67. Joiner ML *et al.* 2012 CaMKII determines mitochondrial stress responses in heart. *Nature* **491**, 269–273. (doi:10.1038/nature11444)
68. Jung DW, Apel L, Brierley GP. 1990 Matrix free Mg^{2+} changes with metabolic state in isolated heart mitochondria. *Biochemistry* **29**, 4121–4128. (doi:10.1021/bi00469a015)
69. Rutter GA, Osbaldeston NJ, McCormack JG, Denton RM. 1990 Measurement of matrix free Mg^{2+} concentration in rat heart mitochondria by using entrapped fluorescent probes. *Biochem. J.* **271**, 627–634. (doi:10.1042/bj2710627)
70. Bauer PJ. 2001 The local Ca^{2+} concentration profile in the vicinity of a Ca^{2+} channel. *Cell Biochem. Biophys.* **35**, 49–61. (doi:10.1385/CBB:35:1:49)
71. Chad JE, Eckert R. 1984 Calcium domains associated with individual channels can account for anomalous voltage relations of CA-dependent responses. *Biophys. J.* **45**, 993–999. (doi:10.1016/S0006-3495(84)84244-7)
72. Tadross MR, Tsien RW, Yue DT. 2013 Ca^{2+} channel nanodomains boost local Ca^{2+} amplitude. *Proc. Natl*

Acad. Sci. USA **110**, 15 794–15 799. (doi:10.1073/pnas.1313898110)

73. Walsh C, Barrow S, Voronina S, Chvanov M, Petersen OH, Tepikin A. 2009 Modulation of calcium signalling by mitochondria. *Biochim. Biophys. Acta* **1787**, 1374–1382. (doi:10.1016/j.bbabio.2009.01.007)
74. Parekh AB. 2011 Decoding cytosolic Ca^{2+} oscillations. *Trends Biochem. Sci.* **36**, 78–87. (doi:10.1016/j.tibs.2010.07.013)
75. Scheitlin CG, Julian JA, Shanmughapriya S, Madesh M, Tsoukias NM, Alevriadou BR. 2016 Endothelial mitochondria regulate the intracellular Ca^{2+} response to fluid shear stress. *Am. J. Physiol. Cell Physiol.* **310**, C479–C490. (doi:10.1152/ajpcell.00171.2015)
76. Demaurex N, Rosselin M. 2017 Redox control of mitochondrial calcium uptake. *Mol. Cell* **65**, 961–962. (doi:10.1016/j.molcel.2017.02.029)
77. Berridge MJ. 2009 Inositol trisphosphate and calcium signalling mechanisms. *Biochim. Biophys. Acta* **1793**, 933–940. (doi:10.1016/j.bbamcr.2008.10.005)
78. Iino M, Endo M. 1992 Calcium-dependent immediate feedback control of inositol 1,4,5-triphosphate-induced Ca^{2+} release. *Nature* **360**, 76–78. (doi:10.1038/360076a0)
79. Miyakawa T, Mizushima A, Hirose K, Yamazawa T, Bezprozvanny I, Kurosaki T, Iino M. 2001 Ca^{2+}-sensor region of IP_3 receptor controls intracellular Ca^{2+} signaling. *EMBO J.* **20**, 1674–1680. (doi:10.1093/emboj/20.7.1674)
80. Palty R *et al.* 2010 NCLX is an essential component of mitochondrial Na^+/Ca^{2+} exchange. *Proc. Natl Acad. Sci. USA* **107**, 436–441. (doi:10.1073/pnas.0908099107)
81. Luongo TS *et al.* 2017 The mitochondrial Na^+/Ca^{2+} exchanger is essential for Ca^{2+} homeostasis and viability. *Nature* **545**, 93–97. (doi:10.1038/nature22082)
82. Ishii K, Hirose K, Iino M. 2006 Ca^{2+} shuttling between endoplasmic reticulum and mitochondria underlying Ca^{2+} oscillations. *EMBO Rep.* **7**, 390–396. (doi:10.1038/sj.embor.7400620)
83. Samanta K, Douglas S, Parekh AB. 2014 Mitochondrial calcium uniporter MCU supports cytoplasmic Ca^{2+} oscillations, store-operated Ca^{2+} entry and Ca^{2+}-dependent gene expression in response to receptor stimulation. *PLoS ONE* **9**, e101188. (doi:10.1371/journal.pone.0101188)
84. Murphy MP. 2009 How mitochondria produce reactive oxygen species. *Biochem. J.* **417**, 1–13. (doi:10.1042/BJ20081386)
85. Brookes PS, Yoon Y, Robotham JL, Anders MW, Sheu SS. 2004 Calcium, ATP, and ROS: a mitochondrial love-hate triangle. *Am. J. Physiol. Cell Physiol.* **287**, C817–C833. (doi:10.1152/ajpcell.00139.2004)
86. Lenaz G. 1998 Role of mitochondria in oxidative stress and ageing. *Biochim. Biophys. Acta* **1366**, 53–67. (doi:10.1016/S0005-2728(98)00120-0)
87. Turrens JF, Boveris A. 1980 Generation of superoxide anion by the NADH dehydrogenase of bovine heart mitochondria. *Biochem. J.* **191**, 421–427. (doi:10.1042/bj1910421)
88. Muller FL, Liu Y, Van Remmen H. 2004 Complex III releases superoxide to both sides of the inner mitochondrial membrane. *J. Biol. Chem.* **279**, 49 064–49 073. (doi:10.1074/jbc.M407715200)
89. Gutteridge JM, Halliwell B. 2000 Free radicals and antioxidants in the year 2000. A historical look to the future. *Ann. N.Y. Acad. Sci.* **899**, 136–147. (doi:10.1111/j.1749-6632.2000.tb06182.x)
90. Csordas G, Renken C, Varnai P, Walter L, Weaver D, Buttle KF, Balla T, Mannella CA, Hajnoczky G. 2006 Structural and functional features and significance of the physical linkage between ER and mitochondria. *J. Cell Biol.* **174**, 915–921. (doi:10.1083/jcb.200604016)
91. Kuster GM *et al.* 2010 Redox-mediated reciprocal regulation of SERCA and Na^+-Ca^{2+} exchanger contributes to sarcoplasmic reticulum Ca^{2+} depletion in cardiac myocytes. *Free Radic. Biol. Med.* **48**, 1182–1187. (doi:10.1016/j.freeradbiomed.2010.01.038)
92. Hawkins BJ *et al.* 2010 S-glutathionylation activates STIM1 and alters mitochondrial homeostasis. *J. Cell Biol.* **190**, 391–405. (doi:10.1083/jcb.201004152)
93. Bansaghi S, Golenar T, Madesh M, Csordas G, RamachandraRao S, Sharma K, Yule DI, Joseph SK, Hajnoczky G. 2014 Isoform- and species-specific control of inositol 1,4,5-trisphosphate (IP_3) receptors by reactive oxygen species. *J. Biol. Chem.* **289**, 8170–8181. (doi:10.1074/jbc.M113.504159)
94. Alansary D, Schmidt B, Dorr K, Bogeski I, Rieger H, Kless A, Niemeyer BA. 2016 Thiol dependent intramolecular locking of orai1 channels. *Sci. Rep.* **6**, 33347. (doi:10.1038/srep33347)
95. Zhou Y, Ramachandran S, Oh-Hora M, Rao A, Hogan PG. 2010 Pore architecture of the ORAI1 store-operated calcium channel. *Proc. Natl Acad. Sci. USA* **107**, 4896–4901. (doi:10.1073/pnas.1001169107)
96. Brigelius-Flohe R, Flohe L. 2011 Basic principles and emerging concepts in the redox control of transcription factors. *Antioxid Redox Signal.* **15**, 2335–2381. (doi:10.1089/ars.2010.3534)
97. Bulua AC, Simon A, Maddipati R, Pelletier M, Park H, Kim KY, Sack MN, Kastner DL, Siegel RM. 2011 Mitochondrial reactive oxygen species promote production of proinflammatory cytokines and are elevated in TNFR1-associated periodic syndrome (TRAPS). *J. Exp. Med.* **208**, 519–533. (doi:10.1084/jem.20102049)
98. Chandel NS, Trzyna WC, McClintock DS, Schumacker PT. 2000 Role of oxidants in NF-κB activation and TNF-α gene transcription induced by hypoxia and endotoxin. *J. Immunol.* **165**, 1013–1021. (doi:10.4049/jimmunol.165.2.1013)
99. Circu ML, Aw TY. 2010 Reactive oxygen species, cellular redox systems, and apoptosis. *Free Radic. Biol. Med.* **48**, 749–762. (doi:10.1016/j.freeradbiomed.2009.12.022)
100. Hughes G, Murphy MP, Ledgerwood EC. 2005 Mitochondrial reactive oxygen species regulate the temporal activation of nuclear factor κB to modulate tumour necrosis factor-induced apoptosis: evidence from mitochondria-targeted antioxidants. *Biochem. J.* **389**, 83–89. (doi:10.1042/BJ20050078)
101. Parthasarathi K, Ichimura H, Quadri S, Issekutz A, Bhattacharya J. 2002 Mitochondrial reactive oxygen species regulate spatial profile of proinflammatory responses in lung venular capillaries. *J. Immunol.* **169**, 7078–7086. (doi:10.4049/jimmunol.169.12.7078)
102. Zhang DX, Gutterman DD. 2007 Mitochondrial reactive oxygen species-mediated signaling in endothelial cells. *Am. J. Physiol. Heart Circ. Physiol.* **292**, H2023–H2031. (doi:10.1152/ajpheart.01283.2006)
103. Anathy V, Aesif SW, Guala AS, Havermans M, Reynaert NL, Ho YS, Budd RC, Janssen-Heininger YM. 2009 Redox amplification of apoptosis by caspase-dependent cleavage of glutaredoxin 1 and S-glutathionylation of Fas. *J. Cell Biol.* **184**, 241–252. (doi:10.1083/jcb.200807019)
104. Anathy V *et al.* 2014 Glutaredoxin-1 attenuates S-glutathionylation of the death receptor fas and decreases resolution of Pseudomonas aeruginosa pneumonia. *Am. J. Respir. Crit. Care Med.* **189**, 463–474. (doi:10.1164/rccm.201310-1905OC)
105. Anathy V, Roberson EC, Guala AS, Godburn KE, Budd RC, Janssen-Heininger YM. 2012 Redox-based regulation of apoptosis: S-glutathionylation as a regulatory mechanism to control cell death. *Antioxid. Redox Signal.* **16**, 496–505. (doi:10.1089/ars.2011.4281)
106. Hawkins BJ, Madesh M, Kirkpatrick CJ, Fisher AB. 2007 Superoxide flux in endothelial cells via the chloride channel-3 mediates intracellular signaling. *Mol. Biol. Cell* **18**, 2002–2012. (doi:10.1091/mbc.E06-09-0830)
107. Soboloff J, Madesh M, Gill DL. 2011 Sensing cellular stress through STIM proteins. *Nat. Chem. Biol.* **7**, 488–492. (doi:10.1038/nchembio.619)
108. Madesh M *et al.* 2009 Execution of superoxide-induced cell death by the proapoptotic Bcl-2-related proteins Bid and Bak. *Mol. Cell. Biol.* **29**, 3099–3112. (doi:10.1128/MCB.01845-08)
109. Peleh V, Cordat E, Herrmann JM. 2016 Mia40 is a trans-site receptor that drives protein import into the mitochondrial intermembrane space by hydrophobic substrate binding. *eLife* **5**, e16177. (doi:10.7554/eLife.16177)
110. Dietl A, Maack C. 2017 Targeting mitochondrial calcium handling and reactive oxygen species in heart failure. *Curr. Heart Fail. Rep.* **14**, 338–349. (doi:10.1007/s11897-017-0347-7)
111. Davidson SM. 2010 Endothelial mitochondria and heart disease. *Cardiovasc. Res.* **88**, 58–66. (doi:10.1093/cvr/cvq195)
112. Angelova PR, Abramov AY. 2016 Functional role of mitochondrial reactive oxygen species in physiology. *Free Radic. Biol. Med.* **100**, 81–85. (doi:10.1016/j.freeradbiomed.2016.06.005)
113. Hempel N, Trebak M. 2017 Crosstalk between calcium and reactive oxygen species signaling in cancer. *Cell Calcium* **63**, 70–96. (doi:10.1016/j.ceca.2017.01.007)

114. Gorlach A, Klappa P, Kietzmann T. 2006 The endoplasmic reticulum: folding, calcium homeostasis, signaling, and redox control. *Antioxid. Redox Signal.* **8**, 1391–1418. (doi:10.1089/ars.2006.8.1391)
115. Davies PF. 1995 Flow-mediated endothelial mechanotransduction. *Physiol. Rev.* **75**, 519–560.
116. Mammoto T, Mammoto A, Ingber DE. 2013 Mechanobiology and developmental control. *Annu. Rev. Cell Dev. Biol.* **29**, 27–61. (doi:10.1146/annurev-cellbio-101512-122340)
117. Langille BL, O'Donnell F. 1986 Reductions in arterial diameter produced by chronic decreases in blood flow are endothelium-dependent. *Science* **231**, 405–407. (doi:10.1126/science.3941904)
118. Caro CG, Fitz-Gerald JM, Schroter RC. 1971 Atheroma and arterial wall shear. Observation, correlation and proposal of a shear dependent mass transfer mechanism for atherogenesis. *Proc. R. Soc. Lond. B* **177**, 109–159. (doi:10.1098/rspb.1971.0019)
119. Zarins CK, Giddens DP, Bharadvaj BK, Sottiurai VS, Mabon RF, Glagov S. 1983 Carotid bifurcation atherosclerosis. Quantitative correlation of plaque localization with flow velocity profiles and wall shear stress. *Circ. Res.* **53**, 502–514. (doi:10.1161/01.RES.53.4.502)
120. Brown AJ, Teng Z, Evans PC, Gillard JH, Samady H, Bennett MR. 2016 Role of biomechanical forces in the natural history of coronary atherosclerosis. *Nat. Rev. Cardiol.* **13**, 210–220. (doi:10.1038/nrcardio.2015.203)
121. Can A, Du R. 2016 Association of hemodynamic factors with intracranial aneurysm formation and rupture: systematic review and meta-analysis. *Neurosurgery* **78**, 510–520. (doi:10.1227/NEU.0000000000001083)
122. Browne LD, Bashar K, Griffin P, Kavanagh EG, Walsh SR, Walsh MT. 2015 The role of shear stress in arteriovenous fistula maturation and failure: a systematic review. *PLoS ONE* **10**, e0145795. (doi:10.1371/journal.pone.0145795)
123. Libby P, Ridker PM, Hansson GK. 2011 Progress and challenges in translating the biology of atherosclerosis. *Nature* **473**, 317–325. (doi:10.1038/nature10146)
124. Asakura T, Karino T. 1990 Flow patterns and spatial distribution of atherosclerotic lesions in human coronary arteries. *Circ. Res.* **66**, 1045–1066. (doi:10.1161/01.RES.66.4.1045)
125. Malek AM, Alper SL, Izumo S. 1999 Hemodynamic shear stress and its role in atherosclerosis. *JAMA* **282**, 2035–2042. (doi:10.1001/jama.282.21.2035)
126. Barakat A, Lieu D. 2003 Differential responsiveness of vascular endothelial cells to different types of fluid mechanical shear stress. *Cell Biochem. Biophys.* **38**, 323–343. (doi:10.1385/CBB:38:3:323)
127. Davies PF, Civelek M, Fang Y, Fleming I. 2013 The atherosusceptible endothelium: endothelial phenotypes in complex haemodynamic shear stress regions *in vivo*. *Cardiovasc. Res.* **99**, 315–327. (doi:10.1093/cvr/cvt101)
128. Glagov S, Zarins C, Giddens DPG, Ku DN. 1988 Hemodynamics and atherosclerosis, insights and perspectives gained from studies of human arteries. *Arch. Pathol. Lab. Med.* **112**, 1018–1031.
129. Secomb TW. 2016 Hemodynamics. *Compr. Physiol.* **6**, 975–1003. (doi:10.1002/cphy.c150038)
130. Bird RB, Stewart WE, Lightfoot EN. 1960 *Transport phenomena*. New York, NY: John Wiley & Sons.
131. Fournier RL. 1998 *Basic transport phenomena in biomedical engineering*. Philadelphia, PA: Taylor & Francis.
132. Truskey GA, Yuan F, Katz DF. 2009 *Transport phenomena in biological systems*, 2nd edn. Upper Saddle River, NJ: Pearson Prentice Hall.
133. Ku DN, Giddens DP, Zarins CK, Glagov S. 1985 Pulsatile flow and atherosclerosis in the human carotid bifurcation. Positive correlation between plaque location and low oscillating shear stress. *Arteriosclerosis* **5**, 293–302. (doi:10.1161/01.ATV.5.3.293)
134. Friedman MH, Brinkman AM, Qin JJ, Seed WA. 1993 Relation between coronary artery geometry and the distribution of early sudanophilic lesions. *Atherosclerosis* **98**, 193–199. (doi:10.1016/0021-9150(93)90128-H)
135. Krams R, Wentzel JJ, Oomen JA, Vinke R, Schuurbiers JC, de Feyter PJ, Serruys PW, Slager CJ. 1997 Evaluation of endothelial shear stress and 3D geometry as factors determining the development of atherosclerosis and remodeling in human coronary arteries *in vivo*. Combining 3D reconstruction from angiography and IVUS (ANGUS) with computational fluid dynamics. *Arterioscler. Thromb. Vasc. Biol.* **17**, 2061–2065. (doi:10.1161/01.ATV.17.10.2061)
136. Dewey CFJ, Bussolari SR, Gimbrone MAJ, Davies PF. 1981 The dynamic response of vascular endothelial cells to fluid shear stress. *J. Biomech. Eng.* **103**, 177–185. (doi:10.1115/1.3138276)
137. Davies PF, Remuzzi A, Gordon EJ, Dewey Jr CF, Gimbrone Jr MA. 1986 Turbulent fluid shear stress induces vascular endothelial cell turnover *in vitro*. *Proc. Natl Acad. Sci. USA* **83**, 2114–2117. (doi:10.1073/pnas.83.7.2114)
138. Hsiai TK, Cho SK, Reddy S, Hama S, Navab M, Demer LL, Honda HM, Ho CM. 2001 Pulsatile flow regulates monocyte adhesion to oxidized lipid-induced endothelial cells. *Arterioscler. Thromb. Vasc. Biol.* **21**, 1770–1776. (doi:10.1161/hq1001.097104)
139. Li YS, Haga JH, Chien S. 2005 Molecular basis of the effects of shear stress on vascular endothelial cells. *J. Biomech.* **38**, 1949–1971. (doi:10.1016/j.jbiomech.2004.09.030)
140. Hsieh HJ, Liu CA, Huang B, Tseng AH, Wang DL. 2014 Shear-induced endothelial mechanotransduction: the interplay between reactive oxygen species (ROS) and nitric oxide (NO) and the pathophysiological implications. *J. Biomed. Sci.* **21**, 3. (doi:10.1186/1423-0127-21-3)
141. Passerini AG *et al.* 2004 Coexisting proinflammatory and antioxidative endothelial transcription profiles in a disturbed flow region of the adult porcine aorta. *Proc. Natl Acad. Sci. USA* **101**, 2482–2487. (doi:10.1073/pnas.0305938101)
142. Civelek M, Manduchi E, Riley RJ, Stoeckert Jr CJ, Davies PF. 2011 Coronary artery endothelial transcriptome *in vivo*: identification of endoplasmic reticulum stress and enhanced reactive oxygen species by gene connectivity network analysis. *Circ. Cardiovasc. Genet.* **4**, 243–252. (doi:10.1161/CIRCGENETICS.110.958926)
143. Nam D, Ni CW, Rezvan A, Suo J, Budzyn K, Llanos A, Harrison D, Giddens D, Jo H. 2009 Partial carotid ligation is a model of acutely induced disturbed flow, leading to rapid endothelial dysfunction and atherosclerosis. *Am. J. Physiol. Heart Circ. Physiol.* **297**, H1535–H1543. (doi:10.1152/ajpheart.00510.2009)
144. Wang C, Baker BM, Chen CS, Schwartz MA. 2013 Endothelial cell sensing of flow direction. *Arterioscler. Thromb. Vasc. Biol.* **33**, 2130–2136. (doi:10.1161/ATVBAHA.113.301826)
145. Feaver RE, Gelfand BD, Blackman BR. 2013 Human haemodynamic frequency harmonics regulate the inflammatory phenotype of vascular endothelial cells. *Nat. Commun.* **4**, 1525. (doi:10.1038/ncomms2530)
146. Bryan MT, Duckles H, Feng S, Hsiao ST, Kim HR, Serbanovic-Canic J, Evans PC. 2014 Mechanoresponsive networks controlling vascular inflammation. *Arterioscler. Thromb. Vasc. Biol.* **34**, 2199–2205. (doi:10.1161/ATVBAHA.114.303424)
147. Levesque MJ, Sprague EA, Nerem RM. 1990 Vascular endothelial cell proliferation in culture and the influence of flow. *Biomaterials* **11**, 702–707. (doi:10.1016/0142-9612(90)90031-K)
148. Dimmeler S, Haendeler J, Rippmann V, Nehls M, Zeiher AM. 1996 Shear stress inhibits apoptosis of human endothelial cells. *FEBS Lett.* **399**, 71–74. (doi:10.1016/S0014-5793(96)01289-6)
149. DePaola N, Gimbrone Jr MA, Davies PF, Dewey Jr CF. 1992 Vascular endothelium responds to fluid shear stress gradients. *Arterioscler. Thromb.* **12**, 1254–1257. (doi:10.1161/01.ATV.12.11.1254)
150. Dai G, Vaughn S, Zhang Y, Wang ET, Garcia-Cardena G, Gimbrone Jr MA. 2007 Biomechanical forces in atherosclerosis-resistant vascular regions regulate endothelial redox balance via phosphoinositol 3-kinase/Akt-dependent activation of Nrf2. *Circ. Res.* **101**, 723–733. (doi:10.1161/CIRCRESAHA.107.152942)
151. Corson MA, James NL, Latta SE, Nerem RM, Berk BC, Harrison DG. 1996 Phosphorylation of endothelial nitric oxide synthase in response to fluid shear stress. *Circ. Res.* **79**, 984–991. (doi:10.1161/01.RES.79.5.984)
152. Dimmeler S, Fleming I, Fisslthaler B, Hermann C, Busse R, Zeiher AM. 1999 Activation of nitric oxide synthase in endothelial cells by Akt-dependent phosphorylation. *Nature* **399**, 601–605. (doi:10.1038/21224)
153. Hwang J, Ing MH, Salazar A, Lassegue B, Griendling K, Navab M, Sevanian A, Hsiai TK. 2003 Pulsatile versus oscillatory shear stress regulates NADPH oxidase subunit expression: implication for native

LDL oxidation. *Circ. Res.* **93**, 1225–1232. (doi:10.1161/01.RES.0000104087.29395.66)

154. Lam CF, Peterson TE, Richardson DM, Croatt AJ, d'Uscio LV, Nath KA, Katusic ZS. 2006 Increased blood flow causes coordinated upregulation of arterial eNOS and biosynthesis of tetrahydrobiopterin. *Am. J. Physiol. Heart Circ. Physiol.* **290**, H786–H793. (doi:10.1152/ajpheart.00759.2005)
155. Ziegler T, Bouzourene K, Harrison VJ, Brunner HR, Hayoz D. 1998 Influence of oscillatory and unidirectional flow environments on the expression of endothelin and nitric oxide synthase in cultured endothelial cells. *Arterioscler. Thromb. Vasc. Biol.* **18**, 686–692. (doi:10.1161/01.ATV.18.5.686)
156. Wu W *et al.* 2011 Flow-dependent regulation of kruppel-like factor 2 is mediated by MicroRNA-92a. *Circulation* **124**, 633–641. (doi:10.1161/CIRCULATIONAHA.110.005108)
157. Sorop O, Spaan JA, Sweeney TE, VanBavel E. 2003 Effect of steady versus oscillating flow on porcine coronary arterioles: involvement of NO and superoxide anion. *Circ. Res.* **92**, 1344–1351. (doi:10.1161/01.RES.0000078604.47063.2B)
158. Phillips SA, Hatoum OA, Gutterman DD. 2007 The mechanism of flow-induced dilation in human adipose arterioles involves hydrogen peroxide during CAD. *Am. J. Physiol. Heart Circ. Physiol.* **292**, H93–H100. (doi:10.1152/ajpheart.00819.2006)
159. Raqeeb A, Sheng J, Ao N, Braun AP. 2011 Purinergic $P2Y_2$ receptors mediate rapid Ca^{2+} mobilization, membrane hyperpolarization and nitric oxide production in human vascular endothelial cells. *Cell Calcium* **49**, 240–248. (doi:10.1016/j.ceca.2011.02.008)
160. Yamamoto K, Furuya K, Nakamura M, Kobatake E, Sokabe M, Ando J. 2011 Visualization of flow-induced ATP release and triggering of Ca^{2+} waves at caveolae in vascular endothelial cells. *J. Cell Sci.* **124**, 3477–3483. (doi:10.1242/jcs.087221)
161. Wang S *et al.* 2015 $P2Y_2$ and G_q/G_{11} control blood pressure by mediating endothelial mechanotransduction. *J. Clin. Invest.* **125**, 3077–3086. (doi:10.1172/JCI81067)
162. Wang W, Ha CH, Jhun BS, Wong C, Jain MK, Jin ZG. 2010 Fluid shear stress stimulates phosphorylation-dependent nuclear export of HDAC5 and mediates expression of KLF2 and eNOS. *Blood* **115**, 2971–2979. (doi:10.1182/blood-2009-05-224824)
163. Fang Y, Davies PF. 2012 Site-specific microRNA-92a regulation of Kruppel-like factors 4 and 2 in atherosusceptible endothelium. *Arterioscler. Thromb. Vasc. Biol.* **32**, 979–987. (doi:10.1161/ATVBAHA.111.244053)
164. Kumar A, Kim CS, Hoffman TA, Naqvi A, Dericco J, Jung SB, Lin Z, Jain MK, Irani K. 2011 p53 impairs endothelial function by transcriptionally repressing Kruppel-like factor 2. *Arterioscler. Thromb. Vasc. Biol.* **31**, 133–141. (doi:10.1161/ATVBAHA.110.215061)
165. Warboys CM *et al.* 2014 Disturbed flow promotes endothelial senescence via a p53-dependent pathway. *Arterioscler. Thromb. Vasc. Biol.* **34**, 985–995. (doi:10.1161/ATVBAHA.114.303415)
166. Shen J, Luscinskas FW, Connolly A, Dewey CFJ, Gimbrone MAJ. 1992 Fluid shear stress modulates cytosolic free calcium in vascular endothelial cells. *Am. J. Physiol.* **262**, C384–C390.
167. James NL, Harrison DG, Nerem RM. 1995 Effects of shear on endothelial cell calcium in the presence and absence of ATP. *FASEB J.* **9**, 968–973.
168. Kwan HY, Leung PC, Huang Y, Yao X. 2003 Depletion of intracellular Ca^{2+} stores sensitizes the flow-induced Ca^{2+} influx in rat endothelial cells. *Circ. Res.* **92**, 286–292. (doi:10.1161/01.RES.0000054625.24468.08)
169. Duza T, Sarelius IH. 2004 Localized transient increases in endothelial cell Ca^{2+} in arterioles in situ: implications for coordination of vascular function. *Am. J. Physiol. Heart Circ. Physiol.* **286**, H2322–H2331. (doi:10.1152/ajpheart.00006.2004)
170. Liu B, Lu S, Zheng S, Jiang Z, Wang Y. 2011 Two distinct phases of calcium signalling under flow. *Cardiovasc. Res.* **91**, 124–133. (doi:10.1093/cvr/cvr033)
171. Yamamoto K, Korenaga R, Kamiya A, Ando J. 2000 Fluid shear stress activates Ca^{2+} influx into human endothelial cells via P2X4 purinoceptors. *Circ. Res.* **87**, 385–391. (doi:10.1161/01.RES.87.5.385)
172. Ando J, Yamamoto K. 2013 Flow detection and calcium signalling in vascular endothelial cells. *Cardiovasc. Res.* **99**, 260–268. (doi:10.1093/cvr/cvt084)
173. Shanmughapriya S *et al.* 2015 Ca^{2+} signals regulate mitochondrial metabolism by stimulating CREB-mediated expression of the mitochondrial Ca^{2+} uniporter gene MCU. *Sci. Signal.* **8**, ra23. (doi:10.1126/scisignal.2005673)
174. Helmlinger G, Berk BC, Nerem RM. 1995 Calcium responses of endothelial cell monolayers subjected to pulsatile and steady laminar flow differ. *Am. J. Physiol.* **269**, C367–C375.
175. Helmlinger G, Berk BC, Nerem RM. 1996 Pulsatile and steady flow-induced calcium oscillations in single cultured endothelial cells. *J. Vasc. Res.* **33**, 360–369. (doi:10.1159/000159164)
176. Prendergast C, Quayle J, Burdyga T, Wray S. 2014 Atherosclerosis differentially affects calcium signalling in endothelial cells from aortic arch and thoracic aorta in apolipoprotein E knockout mice. *Physiol. Rep.* **2**, e12171. (doi:10.14814/phy2.12171)
177. Taylor MS, Choi CS, Bayazid L, Glosemeyer KE, Baker CCP, Weber DS. 2017 Changes in vascular reactivity and endothelial Ca^{2+} dynamics with chronic low flow. *Microcirculation* **24**, e12354. (doi:10.1111/micc.12354)
178. Waldeck-Weiermair M, Alam MR, Khan MJ, Deak AT, Vishnu N, Karsten F, Imamura H, Graier WF, Malli R. 2012 Spatiotemporal correlations between cytosolic and mitochondrial Ca^{2+} signals using a novel red-shifted mitochondrial targeted cameleon. *PLoS ONE* **7**, e45917. (doi:10.1371/journal.pone.0045917)
179. Suzuki J, Kanemaru K, Ishii K, Ohkura M, Okubo Y, Iino M. 2014 Imaging intraorganellar Ca^{2+} at subcellular resolution using CEPIA. *Nat. Commun.* **5**, 4153. (doi:10.1038/ncomms5153)
180. Drago I, De Stefani D, Rizzuto R, Pozzan T. 2012 Mitochondrial Ca^{2+} uptake contributes to buffering cytoplasmic Ca^{2+} peaks in cardiomyocytes. *Proc. Natl Acad. Sci. USA* **109**, 12 986–12 991. (doi:10.1073/pnas.1210718109)
181. Hopkins PN. 2013 Molecular biology of atherosclerosis. *Physiol. Rev.* **93**, 1317–1542. (doi:10.1152/physrev.00004.2012)
182. Chappell DC, Varner SE, Nerem RM, Medford RM, Alexander RW. 1998 Oscillatory shear stress stimulates adhesion molecule expression in cultured human endothelium. *Circ. Res.* **82**, 532–539. (doi:10.1161/01.RES.82.5.532)
183. De Keulenaer GW, Chappell DC, Ishizaka N, Nerem RM, Alexander RW, Griendling KK. 1998 Oscillatory and steady laminar shear stress differentially affect human endothelial redox state. Role of a superoxide-producing NADH oxidase. *Circ. Res.* **82**, 1094–1101. (doi:10.1161/01.RES.82.10.1094)
184. Yeh LH, Park YJ, Hansalia RJ, Ahmed IS, Deshpande SS, Goldschmidt-Clermont PJ, Irani K, Alevriadou BR. 1999 Shear-induced tyrosine phosphorylation in endothelial cells requires Rac1-dependent production of ROS. *Am. J. Physiol.* **276**, C838–C847.
185. Bao X, Lu C, Frangos JA. 2001 Mechanism of temporal gradients in shear-induced ERK1/2 activation and proliferation in endothelial cells. *Am. J. Physiol.* **281**, H22–H29.
186. Han Z, Varadharaj S, Giedt RJ, Zweier JL, Szeto HH, Alevriadou BR. 2009 Mitochondria-derived reactive oxygen species mediate heme oxygenase-1 expression in sheared endothelial cells. *J. Pharmacol. Exp. Ther.* **329**, 94–101. (doi:10.1124/jpet.108.145557)
187. Li JM, Shah AM. 2004 Endothelial cell superoxide generation: regulation and relevance for cardiovascular pathophysiology. *Am. J. Physiol. Regul. Integr. Comp. Physiol.* **287**, R1014–R1030. (doi:10.1152/ajpregu.00124.2004)
188. Sorescu GP *et al.* 2004 Bone morphogenic protein 4 produced in endothelial cells by oscillatory shear stress induces monocyte adhesion by stimulating reactive oxygen species production from a nox1-based NADPH oxidase. *Circ. Res.* **95**, 773–779. (doi:10.1161/01.RES.0000145728.22878.45)
189. Civelek M, Manduchi E, Riley RJ, Stoeckert Jr CJ, Davies PF. 2009 Chronic endoplasmic reticulum stress activates unfolded protein response in arterial endothelium in regions of susceptibility to atherosclerosis. *Circ. Res.* **105**, 453–461. (doi:10.1161/CIRCRESAHA.109.203711)
190. Chaube R, Werstuck GH. 2016 Mitochondrial ROS versus ER ROS: which comes first in myocardial calcium dysregulation? *Front. Cardiovasc. Med.* **3**, 36. (doi:10.3389/fcvm.2016.00036)
191. Beckman JS, Koppenol WH. 1996 Nitric oxide, superoxide, and peroxynitrite: the good, the bad, and ugly. *Am. J. Physiol.* **271**, C1424–C1437.

192. Forstermann U. 2010 Nitric oxide and oxidative stress in vascular disease. *Pflugers Arch.* **459**, 923–939. (doi:10.1007/s00424-010-0808-2)
193. Hsiai TK, Hwang J, Barr ML, Correa A, Hamilton R, Alavi M, Rouhanizadeh M, Cadenas E, Hazen SL. 2007 Hemodynamics influences vascular peroxynitrite formation: implication for low-density lipoprotein apo-B-100 nitration. *Free Radic. Biol. Med.* **42**, 519–529. (doi:10.1016/j.freeradbiomed.2006.11.017)
194. Han Z, Chen YR, Jones 3rd CI, Meenakshisundaram G, Zweier JL, Alevriadou BR. 2007 Shear-induced reactive nitrogen species inhibit mitochondrial respiratory complex activities in cultured vascular endothelial cells. *Am. J. Physiol. Cell Physiol.* **292**, C1103–C1112. (doi:10.1152/ajpcell.00389.2006)
195. Jones 3rd CI, Han Z, Presley T, Varadharaj S, Zweier JL, Ilangovan G, Alevriadou BR. 2008 Endothelial cell respiration is affected by the oxygen tension during shear exposure: role of mitochondrial peroxynitrite. *Am. J. Physiol. Cell Physiol.* **295**, C180–C191. (doi:10.1152/ajpcell.00549.2007)
196. Siu KL, Gao L, Cai H. 2016 Differential roles of protein complexes NOX1-NOXO1 and NOX2-p47phox in mediating endothelial redox responses to oscillatory and unidirectional laminar shear stress. *J. Biol. Chem.* **291**, 8653–8662. (doi:10.1074/jbc.M115.713149)
197. Li X *et al.* 2016 Mitochondrial reactive oxygen species mediate lysophosphatidylcholine-induced endothelial cell activation. *Arterioscler. Thromb. Vasc. Biol.* **36**, 1090–1100. (doi:10.1161/ATVBAHA.115.306964)
198. Verfaillie T *et al.* 2012 PERK is required at the ER-mitochondrial contact sites to convey apoptosis after ROS-based ER stress. *Cell Death Differ.* **19**, 1880–1891. (doi:10.1038/cdd.2012.74)
199. Nussenzweig SC, Verma S, Finkel T. 2015 The role of autophagy in vascular biology. *Circ. Res.* **116**, 480–488. (doi:10.1161/CIRCRESAHA.116.303805)
200. Yan Y, Finkel T. 2016 Autophagy as a regulator of cardiovascular redox homeostasis. *Free Radic. Biol. Med.* **109**, 108–113. (doi:10.1016/j.freeradbiomed.2016.12.003)
201. Bravo-San Pedro JM, Kroemer G, Galluzzi L. 2017 Autophagy and mitophagy in cardiovascular disease. *Circ. Res.* **120**, 1812–1824. (doi:10.1161/CIRCRESAHA.117.311082)
202. Bharath LP *et al.* 2014 Impairment of autophagy in endothelial cells prevents shear-stress-induced increases in nitric oxide bioavailability. *Can. J. Physiol. Pharmacol.* **92**, 605–612. (doi:10.1139/cjpp-2014-0017)
203. Guo F *et al.* 2014 Autophagy regulates vascular endothelial cell eNOS and ET-1 expression induced by laminar shear stress in an ex vivo perfused system. *Ann. Biomed. Eng.* **42**, 1978–1988. (doi:10.1007/s10439-014-1033-5)
204. Li R *et al.* 2015 Disturbed flow induces autophagy, but impairs autophagic flux to perturb mitochondrial homeostasis. *Antioxid. Redox Signal.* **23**, 1207–1219. (doi:10.1089/ars.2014.5896)
205. Galluzzi L, Bravo-San Pedro JM, Levine B, Green DR, Kroemer G. 2017 Pharmacological modulation of autophagy: therapeutic potential and persisting obstacles. *Nat. Rev. Drug Discovery* **16**, 487–511. (doi:10.1038/nrd.2017.22)
206. Lu H, Fan Y, Qiao C, Liang W, Hu W, Zhu T, Zhang J, Chen YE. 2017 TFEB inhibits endothelial cell inflammation and reduces atherosclerosis. *Sci. Signal.* **10**, eaah4214. (doi:10.1126/scisignal.aah4214)